Thermochimica Acta 750 (2025) 180038

Contents lists available at ScienceDirect

Thermochimica Acta

journal homepage: www.elsevier.com/locate/tca

Hierarchical kinetic analysis for development of a reduced-order model of the multi-step thermal decomposition of munitions wastewater

Roshan Adhikari [a,*], Jason Rabinovitch [b], Nick Parziale [b], Christos Christodoulatos [a]

[a] Department of Civil, Environmental and Ocean Engineering, Stevens Institute of Technology, 1 Castle Point Terrace, Hoboken, 07030, NJ, US
[b] Department of Mechanical Engineering, Stevens Institute of Technology, 1 Castle Point Terrace, Hoboken, 07030, NJ, US

ARTICLE INFO

Keywords:
Multi-step kinetics
Hierarchical kinetic analysis
Mathematical deconvolution
Reaction mechanisms
Reduced-order model
Ammonium nitrate wastewater

ABSTRACT

Kinetic modeling of complex, multi-component decomposition processes is typically challenging, and often requires extensive mechanistic knowledge and data from multiple techniques. This work presents a systematic framework to address these challenges, by employing a hierarchical approach to kinetic analysis, applied to experimental data from a single thermoanalytical technique, and without relying on compositional or mechanistic information, to develop an accurate reduced-order model of the thermal decomposition of munitions wastewater at 5 MPa. Composite heat flow signals obtained at 5–20 °C/min were resolved into seven peaks with an iterative deconvolution procedure by leveraging features in the original signals and subsequent residuals. Kinetic parameters for these peaks were estimated with isoconversional analysis and model fitting, refined through ODE optimization, and combined with independently modeled peak weights to construct the reduced-order model. This model was extended into a multi-step model by assigning semi-global reactions to deconvoluted peaks based on alignment with expected reaction behaviors. Both models reproduce experimental conversion profiles with $r^2 \geq 0.996$, demonstrating the method's effectiveness in analyzing highly overlapped multi-step reactions. The methodology presented here offers a framework that could be adapted for effective kinetic analysis of other similarly challenging systems.

1. Introduction

Ammonium nitrate (AN) is used extensively in many propellants and industrial explosives [1–3] due to its high oxygen balance of +20% [4], often leading to AN-laden waste products which require careful disposal measures to mitigate associated environmental risks [5–7]. We discussed one such waste product, called the AN Solution (ANSol) wastewater, and demonstrated the feasibility of energy harvest from its thermal decomposition in our previous work [8]. This wastewater consists of AN, mono-, di-, and tri-methylammonium nitrates (MAN, DMAN, TMAN), and explosives (RDX and HMX), has a gravimetric energy density of 4.07 MJ kg^{-1}, and produces an exhaust stream consisting of 53.7% H_2O, 22% N_2, 12% CO_2, and 12.2% N_2O by mass. The ideal decomposition and the standard enthalpy of reaction of 1 kg of the ANSol wastewater is shown in reaction R1. The standard enthalpy of reaction is calculated from the standard enthalpies of formation of the reactants and products (including enthalpies of solution for dissolved species) using data from [9–13].

$$8.12\,NH_4NO_3\,(aq) + 1.91\,[CH_3NH_3]NO_3\,(aq) + 0.09\,[(CH_3)_2NH_2]NO_3\,(aq) + 0.08\,[(CH_3)_3NH]NO_3\,(aq) + 0.07\,C_3H_6N_6O_6\,(s) + 0.05\,C_4H_8N_8O_8\,(s) + 6.67\,H_2O\,(l) \longrightarrow 2.75\,CO_2\,(g) + 7.84\,N_2\,(g) + 29.84\,H_2O\,(l) + 2.77\,N_2O\,(g), \quad \Delta H^0_{rxn} = -4.07\,MJ/kg \qquad (R1)$$

Large-scale reactors would be required for the thermal destruction of industrial quantities of the ANSol wastewater. However, the composition and energy content of this wastewater means that its treatment in large batch reactors could result in runaway reactions, due to a low cooling number associated with these reactors [14]. Therefore, continuous decomposition in a flow reactor is a lower-risk experimental approach when investigating the scalability of utilizing the ANSol wastewater as a fuel. Such a scale-up would benefit from a theoretical tool capable of predicting the wastewater conversion across the reactor's operation parameter space. Accordingly, this work aims to develop a reduced-order model of the ANSol wastewater decomposition as a theoretical tool to inform and complement experimental works in a flow reactor.

Detailed reaction kinetics simulation of the munitions wastewater decomposition using tools such as CHEMKIN [15] and Cantera [16] can provide important insights into the decomposition process and

* Corresponding author.
E-mail address: radhikari.acad@gmail.com (R. Adhikari).

https://doi.org/10.1016/j.tca.2025.180038
Received 17 February 2025; Received in revised form 27 April 2025; Accepted 21 May 2025
Available online 10 June 2025

chemical pathways. However, the presence of multiple reactants, including AN, MANs, and explosives, and the inevitable production of numerous intermediates, makes such simulation of the wastewater decomposition challenging, and will likely require integrating multiple reaction mechanisms, as done by Mosevitzky et al. [17] for combustion simulations of urea and AN fuel. An additional challenge is that the exact composition of the ANSol wastewater can vary according to upstream products and processes [8], and it is desirable to apply the thermal destruction treatment to wastewaters of varying compositions in a production-level setting.

While all species in the wastewater contain oxygen, we consider AN, the only species with a positive oxygen balance in the mixture, to act as the oxidizer for the other "fuel" species. It is therefore reasonable to assume that the wastewater decomposition consists of multiple reactions competing over the oxidizing species produced from AN, primarily via either an ionic dissociation [18], or a radical decomposition [19]. Moreover, the DSC curves of the wastewater decomposition we reported in [8] showed distinct features at or immediately following the decomposition temperatures of the fuel species, suggesting consecutive reactions driving the decomposition process. Overall, the wastewater decomposition is a complex process with many non-independent reactions, which makes it particularly challenging to model this process with traditional kinetic analysis techniques.

Techniques typically used for kinetic analysis of thermoanalytical signals are based on the rate equation for single-step reactions [20,21]. Application of these techniques to complex reactions consisting of independent steps is usually straightforward, but kinetic analysis of complex reactions with non-independent steps is challenging [22–24]. Some examples of these challenges include: (a) identifying the correct number of rate-limiting steps and their reaction models [25,26], (b) obtaining independent mechanistic information to determine reaction steps and models in case of significant overlapping [20], (c) obtaining reliable initial values for model parameters via physicochemical and microscopic techniques [27], (d) separating thermal effects with oppositely signed thermoanalytical signals [28,29], (e) selecting from a very large number of candidate model combinations when the number of rate-limiting steps constituting the complex process increase [30], and (f) implementing non-linear regression approaches [20] that are computationally expensive and difficult [31].

Nevertheless, the importance of rigorous solutions of the kinetics of complex processes for many practical purposes [28] has inspired multiple works with various approaches to the problem [22,26–28,32–41]. Many studies typically utilize multiple techniques of thermal analysis and material characterization to aid in developing multi-step kinetic models of complex reactions [42–45]. One noteworthy point about these works is that they typically deal with thermoanalytical signals comprising two to four peaks, some of which are distinct due to a low degree of overlapping. In contrast, the munitions wastewater has six reacting species excluding water (reaction R1), one of which is considered to be the oxidizer, and the others are considered to be the fuel species. Therefore, the decomposition process consists of at least five semi-global reactions. Moreover, as shall be seen later, the signals representing "pseudo-reactions" in the DSC heat flow curves of the wastewater decomposition are highly overlapped, making kinetic analysis even more complicated.

To address these challenges in modeling the wastewater decomposition, we employ a systematic hierarchical approach to kinetic analysis, aiming to develop a predictive reduced-order model of the decomposition process without considering the sample composition or the reaction pathways. In addition, we aim to develop a generalized computation procedure that can be applied to obtain similar models for wastewater streams of varying compositions, or for decomposition under different thermal loads. Overall, our focus is on developing robust empirical models for predictive purposes, rather than extracting fundamental kinetic parameters. Therefore, the reduced-order model is developed from kinetic analysis of DSC heat flow signals alone, simplifying data collection for future applications to diverse streams. First, we sequentially employ mathematical deconvolution, isoconversional analysis, model fitting, and ODE optimization of kinetic parameters to develop the reduced-order model. Thereafter, a comprehensive multi-step model that can consider interactions between different reactions [20] is developed by supplementing the reduced-order model with mechanistic information regarding the sample composition and semi-global reactions comprising the decomposition process.

Table 1
Species and elemental composition of the Final Sludge munitions wastewater.

Species	Mass %	Elements	Mass %
Ammonium Nitrate (AN)	65	Carbon	3.4
Methylammonium Nitrate (MAN)	18	Hydrogen	6.1
Water	12	Nitrogen	29.4
Dimethylammonium nitrate (DMAN)	1	Oxygen	61.1
Trimethylammonium nitrate (TMAN)	1		
Explosives (RDX and HMX)	3		

2. Materials and methods

An overview of the method used in this work is illustrated in Fig. 1.

2.1. Sample material

A type of munitions wastewater called the final sludge (FS) ANSol wastewater was obtained from an industrial munitions plant. The composition of this wastewater, by mass percentages of constituting species and elements, is provided in Table 1.

2.2. Thermal analysis

Thermal analysis of the wastewater decomposition was performed in a High-Pressure Differential Scanning Calorimeter (HP DSC 2+) from Mettler Toledo, calibrated for heat flow and temperature measurements with zinc and indium. The procedure for this analysis is similar to what we used in our previous work [8], except using smaller sample masses and lower purge gas flow rates in this work. Before sample preparation, the sample container was submerged in a water bath at 80 °C for two hours to prevent precipitation of AN and MANs and obtain a homogeneous mixture. Small samples of masses between 3 to 4 mg were prepared in standard 40 μL aluminum crucibles with approximately 0.5 mm diameter holes in the lids. The small sample size ensures uniform temperature distribution in the sample and prevents self-heating [25,46]. Experiments were performed under an inert research grade N_2 environment at 5 MPa pressure, and evolved gaseous species were purged out of the DSC with a 50 mL/min flow of N_2. The selected pressure is representative of the operating pressure of a continuous flow reactor for thermal destruction of the wastewater. The basis for this selection is our prior work in analyzing the FS wastewater decomposition, where experiments above 5 MPa resulted in minimal increases in enthalpy release, and small further decreases in quantities of harmful gases [8]. Similar trends in quantities of pollutant gases were also found in an analysis of urea and ammonium nitrate (UAN) fuel by Dana et al. [47,48].

The sample was heated from 40 °C to 400 °C at four different heating rates of 5, 10, 15, and 20 °C/min. The use of multiple heating rates follows the recommendations of the ICTAC kinetics committee for kinetic analysis using nonisothermal methods [25,49,50]. All DSC curves of the wastewater decomposition were blank-corrected before further analysis, and the decomposition enthalpies were determined from the areas between the exothermic segments and appropriately selected spline baselines.

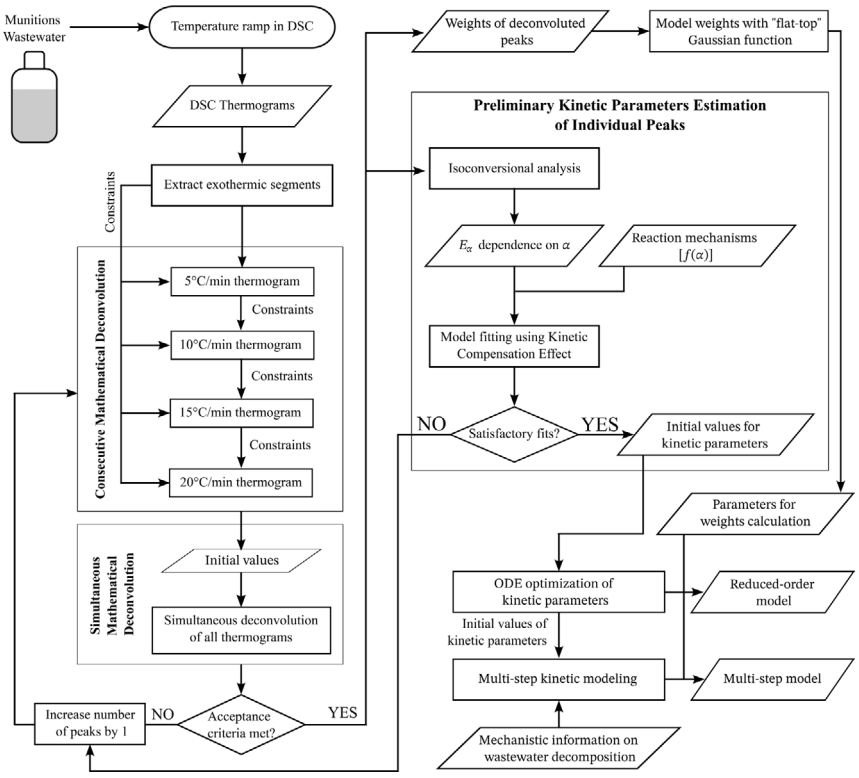

Fig. 1. Flowchart of the hierarchical approach to kinetic analysis for development of predictive reduced-order and multi-step models of the complex munitions wastewater decomposition process.

The DSC curves of the wastewater decomposition show a broad endothermic peak from water vaporization, followed by an exothermic decomposition of the sample. Modeling the entire process would require treating these opposing effects separately, as directly combining them would result in negative conversions during the initial endothermic stage. Therefore, in the reduced-order model, we focus on modeling the decomposition process represented by the exothermic segments of the DSC curves. We then develop a multi-step model, in which water effects are considered through separate expressions for the vaporization and removal of water, and for the inhibition of sample decomposition due to water content. In both models, ODE simulations are initiated well before the experimental onset of decomposition, ensuring that the effects of water content on sample decomposition are incorporated in our kinetic solutions.

2.3. Multi-step kinetic analysis

Kinetic analysis is concerned with the rate of chemical reactions, and the measurement and parameterization of chemical process rates [25,51]. In condensed phase and heterogeneous kinetics, the rate equation is often expressed in terms of conversion (α) as shown in Eq. (1) [52].

$$\frac{d\alpha}{dt} = k(T)f(\alpha) \tag{1}$$

The reaction rate $d\alpha/dt$ also depends on the pressure [25,50,53], but this dependence is ignored in this work since all experiments were carried out at the same pressure. The rate constant $k(T)$ is almost always interpreted in terms of the Arrhenius equation [54], which results in the reaction rate equation being expressed as Eq. (2).

$$\frac{d\alpha}{dt} = A\exp\left(\frac{-E_\alpha}{RT}\right)f(\alpha) \tag{2}$$

Here, A, E_α, and $f(\alpha)$ represent the pre-exponential factor, activation energy, and the reaction model, respectively. Together, these terms are called the kinetic triplets, and kinetic analysis aims to determine these triplets for a single-step reaction, or multiple sets of these triplets for complex multi-step reactions [25]. For complex reactions, the overall conversion and reaction rate are given as the sum of individual conversions and reaction rates as shown in Eqs. (3) and (4), where w_i represents the weights or contributions of individual reactions [20,28].

$$\alpha = \sum_i w_i\alpha_i, \qquad \sum_i w_i = 1 \tag{3}$$

$$\frac{d\alpha}{dt} = \sum_i w_i\frac{d\alpha_i}{dt} = \sum_i w_i A_i \exp\left(\frac{-E_{\alpha,i}}{RT_i}\right)f_i(\alpha), \qquad \sum_i w_i = 1 \tag{4}$$

In this work, the strategy for multi-step kinetic analysis of the munitions wastewater decomposition is to determine n sets of kinetic triplets, where n is the fewest number of pseudo-reactions required to reproduce the composite $d\alpha/dt$ profiles of the wastewater decomposition, according to Eqs. (3) and (4). This strategy of using as few individual steps as possible is consistent with the recommendations of the ICTAC kinetics committee [20] for multi-step analysis of complex processes.

We first resolve the experimental exotherms into n peaks with mathematical deconvolution (Section 2.3.1), and require that the coefficient of determination (r^2) between the experimental data and the sum of deconvoluted peaks is equal to or greater than 0.95. Subsequently, we determine the kinetic triplets of the individual peaks via isoconversional analysis and model fitting (Sections 2.3.2 and 2.3.3), and require that each peak be fitted by a reaction model with $r^2 \geq 0.95$. While r^2 is typically used for evaluating linear regression models rather than for non-linear curve fitting and kinetic predictions, we report these following the recommendations of the ICTAC kinetics committee [20]. Therefore, we also rely on visual inspection of the fits to evaluate the performance of our modeling approach.

2.3.1. Mathematical deconvolution

We perform mathematical deconvolution on the exothermic segments of the DSC curves of the wastewater decomposition to break

down the composite exotherms into n individual peaks, each expressed by a mathematical function, as shown in Eq. (5).

$$\frac{dH}{dt} = \sum_{i=1}^{n} F_i(t) \tag{5}$$

The rationale underlying this approach is the assumption that the overall exothermic segment is composed of multiple pseudo-reactions that together yield the observed heat flow rate (dH/dt) curves and the total enthalpy (ΔH_{tot}), as shown in Eqs. (6) and (7).

$$\frac{dH}{dt} = \sum_{i=1}^{n} \frac{dH_i}{dt} \tag{6}$$

$$\Delta H_{tot} = \sum_{i=1}^{n} \Delta H_i \tag{7}$$

In kinetic analysis of heat flow signals, the conversion and reaction rate for a process are obtained by normalizing the mass-specific partial heat of reaction $\Delta H(t)$ and instantaneous heat flow rate $dH(t)/dt$ by the total heat of reaction (ΔH_{tot}), as shown in Eqs. (8) and (9) respectively [55,56].

$$\alpha = \frac{\Delta H(t)}{\Delta H_{tot}} \tag{8}$$

$$\frac{d\alpha}{dt} = \frac{1}{\Delta H_{tot}} \frac{dH}{dt} \tag{9}$$

Similarly, the reaction rate of a deconvoluted peak can be expressed as:

$$\frac{d\alpha_i}{dt} = \frac{1}{\Delta H_i} \frac{dH_i}{dt} \tag{10}$$

The overall reaction rate in Eq. (9) can be expressed in terms of deconvoluted peaks by substituting the expression for dH/dt from Eq. (6):

$$\frac{d\alpha}{dt} = \frac{1}{\Delta H_{tot}} \sum_{i=1}^{n} \frac{dH_i}{dt} \tag{11}$$

Expressing dH_i/dt in terms of $d\alpha_i/dt$ in Eq. (11) gives:

$$\frac{d\alpha}{dt} = \frac{1}{\Delta H_{tot}} \sum_{i=1}^{n} \Delta H_i \frac{d\alpha_i}{dt} = \sum_{i=1}^{n} \frac{\Delta H_i}{\Delta H_{tot}} \frac{d\alpha_i}{dt} \tag{12}$$

Comparing Eq. (12) with Eq. (4) shows that our approach is equivalent to an alternative approach of performing deconvolution on the $d\alpha/dt$ curves, but provides reliable estimates for the weight of each deconvoluted peak as its contribution to the total measured enthalpy ($w_i = \Delta H_i/\Delta H_{tot}$). Calculating weights through deconvolution of the dH/dt curves is a feature of our hierarchical approach that reduces the number of parameters that need to be optimized simultaneously, and eliminates the need to assume potentially unreliable estimates for the weight parameters. Furthermore, simultaneous optimization of weights often requires imposing non-linear constraints so that Eq. (3) is satisfied, which adds to the complexity and computational expenditure of the optimization process.

We use the Fraser-Suzuki function [57,58] as the mathematical function $F_i(t)$ in Eq. (5) for its asymmetry parameter, since reaction rate curves generally have asymmetric shapes [59], and because it has been reported to fit different reaction rate profiles better than other functions and yield correct kinetic parameters in subsequent kinetic analysis [32]. The mathematical expression of the Fraser-Suzuki function is provided in Eq. (13), where, parameters a, p, w, and s represent the peak's amplitude, position, half-width, and shape (asymmetry) respectively, and T represents the temperature.

$$F(t) = a \exp\left[-\ln 2\left[\frac{\ln\left(1 + 2s\frac{T-p}{w}\right)}{s}\right]^2\right] \tag{13}$$

Our systematic approach to mathematical deconvolution is an iterative process comprising the steps listed below. This approach is illustrated in Fig. 2, which shows its application to the exotherm at the lowest heating rate of 5 °C/min. While acceptable r^2 values (≥ 0.95) for fits between the experimental exotherm and the sum of deconvoluted peaks were achieved with 5 and 6 peaks, the criterion of $r^2 \geq 0.95$ for fits between deconvoluted peaks and reaction model fits was achieved with seven peaks. Therefore, Fig. 2 shows the mathematical deconvolution with seven peaks, which satisfied both acceptance criteria.

1. Inflection points (locations of local maximum heat flow) were identified in the composite exotherm obtained at the lowest heating rate (5 °C/min) by visual inspection. Each inflection point was considered to be the position of an individual peak, and initial guesses for its Fraser-Suzuki parameters a, p, w, and s were determined manually to roughly fit the composite peak. The half-width parameter (w) was made as large as reasonably possible to keep the number of deconvoluted peaks to a minimum.
2. The residual obtained by subtracting the sum of individual peaks from the composite peak was observed to identify the presence and positions of additional peaks, if any. Initial guesses for the Fraser-Suzuki parameters were determined manually again. This iterative process was repeated until the residual no longer exhibited distinct peak-like features and consisted only of random signals.
3. Parameters a, p, w, and s for all peaks were simultaneously optimized with the interior-point algorithm [60] in Matlab. The constraints were chosen based on observation of the experimental exothermic segment. Specifically, the limits for the position parameters were determined from the onset and endset temperatures of the exotherm, while those for the amplitude parameters were set to zero and the maximum heat flow rate in the experimental data. The limits for the width and shape parameters were set to ensure that the peaks would not extend beyond the range of the experimental exotherm. Therefore, the imposed constraints were broad enough to prevent incorrect values without forcing the solutions within an overly narrow basin. The objective function of this optimization was the root mean square error (RMSE) as shown in Eq. (14).

$$RMSE_j = \sqrt{\frac{1}{P}\sum_{k=1}^{P}\left[\left(\frac{dH}{dt}\right)_{exp,j,k} - \left(\frac{dH}{dt}\right)_{fit,j,k}\right]^2} \tag{14}$$

Here, k and P represent the index and total number of data points in the experimental and fitted curves, respectively, and j represents the heating rate. The fitted heat flow curve $(dH/dt)_{fit}$ is the sum of all deconvoluted peaks, as shown in Eq. (15), where i is the index of the deconvoluted peaks.

$$\left(\frac{dH}{dt}\right)_{fit} = \sum_{i=1}^{n}\left(\frac{dH_i}{dt}\right)_{fit} \tag{15}$$

4. Step 3 was then repeated on the exotherms obtained at the higher heating rates (10, 15, and 20 °C/min), one at a time, with the same number of peaks. For each peak, optimized values for the position and amplitude parameters from the lower heating rate program were set as the lower bounds because the exotherms of the wastewater decomposition shift to higher temperatures and are taller at higher heating rates. This behavior is to be expected in kinetic analysis [25], particularly for the range of temperature ramps used in this work. The upper bounds for these parameters were chosen based on observation of the corresponding heat flow rate curves. The half-width and shape parameters were allowed to deviate ±10% and ±3%, respectively, from the optimized values obtained for the lower heating rate data. This is expected to account for changes in how corresponding pseudo-reactions progress at different heating rates due to mutual interactions, which is ignored by mathematical deconvolution [20].

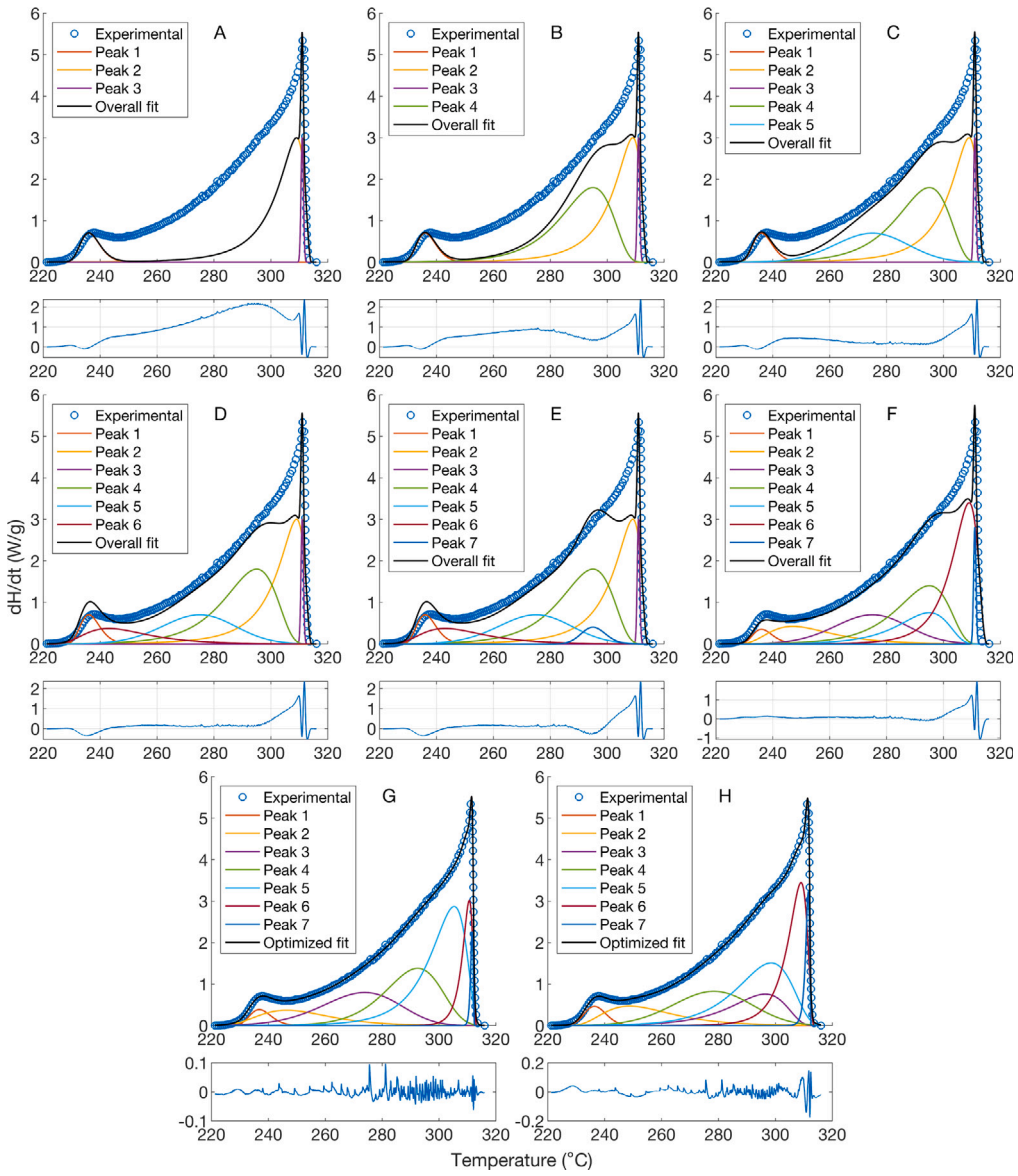

Fig. 2. Illustration of the mathematical deconvolution procedure on the composite exotherm at 5 °C/min: (A-F) Manual exploration and adjustment, and (G) optimization of the number of peaks and corresponding Fraser-Suzuki parameters (steps 1 to 3); (H) final optimization of the Fraser-Suzuki parameters with conversion-related penalties (step 5) that satisfied the acceptance criterion between deconvoluted peaks and empirical model fits (step 6).

5. The Fraser-Suzuki function parameters of all peaks at different heating rates, optimized consecutively as described in steps 3 and 4, were further optimized simultaneously with Matlab's global search function using the interior-point algorithm [60] for local optimization. At this step, the conversion curves of each peak at all heating rates were determined as part of the optimization. In kinetic analysis, these curves are expected to shift to higher temperatures at higher heating rates without intersecting, and as discussed in the previous point, this behavior is especially pertinent to our study. Therefore, penalties, in the form of large values, were added to the objective function if these conditions were not satisfied. The objective function at this step is the sum of RMSE values at individual heating rates, shown in Eq. (14). This optimization procedure resulted in overall fits with r^2 values exceeding 0.95, meeting our acceptance criterion for deconvolution results.
6. The kinetic triplets of deconvoluted peaks were determined as outlined in Sections 2.3.2 and 2.3.3, and the r^2 values of fits between deconvoluted peaks and their reaction model fits were analyzed. Any peak with unsatisfactory fits, based on visual inspection and coefficient of determination (r^2) below 0.95, was further resolved into two peaks, and the whole process was repeated until this criterion was met.

2.3.2. Isoconversional analysis

Isoconversional methods for kinetic analysis are based on the assumption that the reaction rate at any extent of conversion depends only on the temperature, which allows determining the activation energy of the reaction without any knowledge or assumptions about the governing reaction mechanism(s) [25]. We use the differential isoconversional method of Friedman [61] to determine the isoconversional activation energy (E_α) of the mathematically deconvoluted peaks. This method is based on Eq. (16) which is obtained by applying the isoconversional principle to the reaction rate Eq. (9). Using this method, the activation energies at different extents of conversion (E_α) are obtained from the slopes of the plots of $\ln(d\alpha/dt)_{\alpha,j}$ against $1/T_{\alpha,j}$.

$$\ln\left(\frac{d\alpha}{dt}\right)_{\alpha,j} = \ln\left[f(\alpha)A_\alpha\right] - \frac{E_\alpha}{RT_{\alpha,j}} \tag{16}$$

Here, j represents the indices of the temperature ramps used in thermal analysis. When nonisothermal methods, such as constant heating rate programs, are used, it is common to use Friedman method as in Eq. (16) [24,28,36,62], and in a slightly different form that includes the heating rate (β) as well [25,26,33]. In this work, we use Eq. (16) since it allows the use of actual sample temperature instead of the reference temperature if available [25]. However, we use the reference temperature for our modeling due to the difficulty of accurately determining the actual sample temperature during exothermic decomposition.

We choose the Friedman method for isoconversional analysis since it is appropriate for differential signals such as DSC data, and does not rely on approximations and assumptions, unlike many integral methods used in kinetic analysis [25]. While the difficulties in correctly determining the baseline in differential data can result in inaccuracies [63], this limitation would apply to both differential and integral methods in this work, since kinetic analysis is performed on exothermic segments obtained by removing the baseline from experimental curves.

2.3.3. Pre-exponential factor and reaction model

The variation in E_α with conversion of individual peaks deconvoluted in this work indicates that these peaks cannot be considered effectively "single-step", as the acceptance criterion is based on fits with empirical reaction models rather than constancy of E_α. This characteristic makes the master plot method [64], widely used for determining the pre-exponential factor and the reaction mechanism, unsuitable for further analysis in our case. Therefore, we employ the kinetic compensation effect (KCE), a frequently observed phenomenon in kinetic analysis that manifests as a linear relationship between $\ln(A)$ and E_α of a process determined from different approaches, as shown in Eq. (17). Expressing A in terms of E_α, which is determined using the Friedman method, allows fitting of various reaction models to the experimental data, or deconvoluted peaks in this case.

$$\ln(A_\alpha) = aE_\alpha + b \tag{17}$$

The occurrence of KCE has been ascribed to random errors in kinetic measurements [65], or to the selection of incorrect reaction models or inappropriate computation techniques [27], or to the exponential form of the rate constant [66]. Since our work is focused on reproducing the experimentally observed exothermic decomposition behavior of the munitions wastewater, we can employ Eq. (17) to simultaneously obtain A and $f(\alpha)$. To do this, the rate equation for each deconvoluted peak i is expressed as shown in Eq. (18).

$$\frac{d\alpha_i}{dt} = \left[\exp(aE_{\alpha,i} + b)\right] \exp\left(\frac{-E_{\alpha,i}}{RT}\right) f_i(\alpha) \tag{18}$$

Parameters a and b that govern A are influenced by the selection of the reaction model $f(\alpha)$, for which we consider both mechanistic and empirical models. The mechanistic models are included solely as empirical fitting functions, with no mechanistic interpretation implied, and the empirical models are considered since they are likely to fit deconvoluted peaks better. Accordingly, twenty-seven mechanistic models of different types (order of reaction, diffusion, nucleation, and geometric contraction models) compiled by Açıkalın [67] were used. The empirical reaction models considered include nth order reaction model (Eq. (19)) [25], Šesták-Berggren model (Eq. (20)) [68], two variations of truncated Šesták-Berggren model (Eqs. (21) and (22)) [69], introduced by Akulov [70], and also referred to as the extended Prout-Tompkins model [25], nucleation-growth Johnson-Mehl-Avrami-Kolmogorov (JMAK) model (Eq. (23)) [71], and nth order reaction model with autocatalysis (Eq. (24)) [72].

$$f(\alpha) = (1-\alpha)^n \tag{19}$$

$$f(\alpha) = \alpha^m\ (1-\alpha)^n\ [-\ln(1-\alpha)]^p \tag{20}$$

$$f(\alpha) = c\ \alpha^m(1-\alpha)^n \tag{21}$$

$$f(\alpha) = \alpha^m(1-\alpha)^n \tag{22}$$

$$f(\alpha) = m\ (1-\alpha)[-\ln(1-\alpha)]^{1-1/m} \tag{23}$$

$$f(\alpha) = (1-\alpha)^n(1-K\alpha) \tag{24}$$

The parameters governing the reaction rate, as expressed in Eq. (18), include parameters a and b when using mechanistic models, and parameters c, K, m, n, and p in addition when using empirical models. These parameters were determined by constrained optimization of the RMSE between deconvoluted and fitted curves for each peak individually, as shown in Eq. (25), where i, j, and k are indices of the deconvoluted peaks, heating rates, and the data points, respectively. Optimization was performed in Matlab using the interior-point algorithm [60]. For mechanistic models, local optimization was found to be sufficient, while global optimization was necessary for the empirical models due to the higher number of variables to be optimized.

$$RMSE_i = \sum_{j=1}^{M}\left[\sqrt{\frac{1}{P}\sum_{k=1}^{P}\left[\left(\frac{d\alpha}{dt}\right)_{deconv,i,k} - \left(\frac{d\alpha}{dt}\right)_{fit,i,k}\right]^2}\right] \tag{25}$$

As part of the hierarchical approach in building the reduced-order model, this step focused on identifying promising reaction models and initial values of corresponding parameters with simple procedures for a more rigorous treatment afterward. First, the temperature dependence of conversion ($\alpha - T$) of deconvoluted peaks is imposed on the fitted reaction rate peaks ($d\alpha/dt$) in Eq. (25), instead of allowing such dependence to evolve by solving the corresponding differential equations, which is significantly more computationally expensive. In addition, parameters for each peak and reaction model combination were first optimized independently to avoid the large number of model combinations encountered when solving all peaks simultaneously. For each peak, the reaction model that produced the best fit, based on RMSE and r^2 values, and visual inspection, was determined to be the governing mechanism of the pseudo-reaction it represents for further refinement.

2.3.4. ODE optimization of kinetic parameters

To develop the reduced-order model of the wastewater decomposition, the kinetic triplets of each peak determined so far were refined further with ODE optimization. The weights of deconvoluted peaks are modeled independently and combined with the refined kinetic parameters (Section 3.4) to obtain the reduced-order model predictions of the overall process.

The activation energies of the deconvoluted peaks were initially estimated in Section 2.3.2 by enforcing the temperature dependence of conversion. While effective for generating initial values, this approach can introduce discrepancies during ODE simulations, making further refinement necessary. As noted earlier in Section 2.3.3, and discussed in detail later in Section 3.2, E_α varies significantly with conversion for most peaks, and this variation strongly influences the peaks' shapes. To account for this, we scale the E_α of each peak as a multiple of its isoconversional value (Eq. (26)), which allows us to adjust E_α values to improve agreement between simulated and deconvoluted peaks.

$$E_{\alpha,i,new} = f\ E_{\alpha,i} \tag{26}$$

Thereafter, A was expressed in terms of the adjusted E_α (Eq. (27)), and the reaction rate of each peak was expressed as in Eq. (28).

$$\ln(A_{\alpha,i}) = a\ E_{\alpha,i,new} + b = a(f\ E_{\alpha,i}) + b \tag{27}$$

$$\frac{d\alpha_i}{dt} = \exp\left[a(f\ E_{\alpha,i}) + b\right] \exp\left(\frac{-f\ E_{\alpha,i}}{RT}\right) f_i(\alpha) \tag{28}$$

Parameters a, b, f, and a combination of c, K, m, n, and p depending on the peak's empirical reaction model, were optimized separately by minimizing the RMSE error between the deconvoluted and simulated

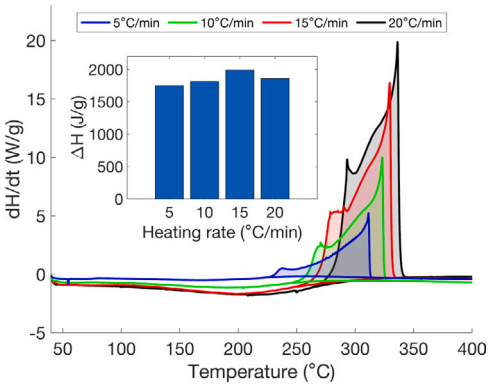

Fig. 3. DSC curves of wastewater decomposition at different heating rates with their corresponding baselines that include the endothermic segments, and *(Inset)* enthalpies of the exothermic segments highlighted by the shaded areas. Data is for experiments at 5 MPa pressure.

curves at all heating rates. The expression for this is similar to the one shown in Eq. (25). In addition, the initial conversions (α_0) for all peaks were also optimized, constrained between bounds of $1e-12$ and $1e-2$. The simulation was performed in Matlab using the forward Euler method with adaptive time stepping, which, for this work, was found to be on par or better than Matlab's higher-order stiff ODE solvers in terms of convergence and stability. The optimization was performed by employing constrained Nelder–Mead [73] and pattern search [74,75] methods in tandem. Both methods navigate to promising regions from initial values using derivative-free methods, and were found to be superior to gradient-descent and stochastic global search methods for this problem.

3. Results and discussions

3.1. Thermal decomposition

Fig. 3 shows the blank-corrected DSC curves of the final sludge munitions wastewater decomposition under 5 MPa nitrogen pressure at different heating rates. The enthalpies of the exothermic segments, highlighted by shaded regions, are also shown.

The T_{onset} of the exotherms shifts to higher values with increasing heating rates, a phenomenon frequently reported in the literature [28,55,76,77]. This shift is primarily due to kinetic limitations, as higher temperatures are required for the reaction to reach the same conversion under faster heating ramps. A smaller contribution may also come from thermal lag, as the sample's thermal properties differ from those of the calibration standards. Additionally, the initial stages of the exotherms become more distinct at higher rates, highlighting the increased prominence of faster reactions during early decomposition.

Total enthalpies (ΔH_{tot}) of the exotherms vary from 1750 J/g at 5 °C/min to 1990 J/g at 15 °C/min. The difference between the highest and lowest values is therefore about 13%, which is reasonable in DSC analysis, and is typically due to heat transfer limitations that are more pronounced at higher heating rates [49]. In this case, however, the complex nature of the wastewater decomposition contributes additional underlying reasons for this phenomenon. First, the decomposition of AN and its mixtures is influenced by gaseous intermediates via heterogeneous catalysis of the condensed phase, or via homogeneous reactions in the gas phase [19,78–81]. Secondly, a significant fraction of the decomposition enthalpy is lost with gaseous intermediates and products, and is not measured by the DSC [8,82,83] – the primary reason why measured ΔH_{tot} values are lower than the ΔH^0_{rxn} for reaction R1. Experimental ΔH_{tot} values in this work are therefore governed by an intricate mechanism encompassing accumulation and loss of reactive intermediates, and loss of sensible heat. Nevertheless, the exotherms have similar profiles and spans at all heating rates, and the variation in enthalpies is reasonable, and we consider the experimental results to be reliable for further kinetic analysis.

Table 2
Minimum, average and maximum values of E_α for deconvoluted peaks for $0.1 < \alpha < 0.9$, and difference between $E_{\alpha,max}$ and $E_{\alpha,min}$ as percentage of $E_{\alpha,avg}$ in this range.

Peak	$E_{\alpha,min}$ (kJ/mol)	$E_{\alpha,avg}$ (kJ/mol)	$E_{\alpha,max}$ (kJ/mol)	$E_{\alpha,diff}$ (%)
1	58.5	63.99	68.86	16.2
2	75.70	77.81	84.39	11.2
3	195.44	206.42	209.83	7.0
4	130.94	139.25	145.14	10.2
5	123.59	139.56	158.95	25.3
6	145.50	168.14	191.63	27.4
7	201.55	212.04	220.63	9.0

3.2. Mathematical deconvolution and isoconversional analysis

Following the procedures outlined in Section 2.3, the composite exotherms at all heating rates were deconvoluted into seven peaks, which are shown in Fig. 4. The deconvolution results are excellent ($r^2 \geq 0.999$), and the residuals are close to zero except for certain segments with noise.

The enthalpy of each peak (ΔH_i) is calculated from the area under its curve, and Fig. 5 shows the enthalpies of all deconvoluted peaks at different heating rates. While the total enthalpy of the overall exotherm remains fairly consistent at all heating rates (Fig. 3), the individual enthalpies of deconvoluted peaks vary, some by large margins. Nevertheless, clear trends emerge in these variations. It is likely that allowing small variations in the width and shape parameters of the deconvoluted peaks at different temperature ramps has allowed the deconvolution procedure to account for heating rate-induced changes to the pseudo-reactions represented by these peaks, which is typically not the case with this procedure [20].

The reaction rate ($d\alpha/dt$) and conversion (α) curves of all deconvoluted peaks are shown in Figs. 6 and 7 respectively. As expected, the conversion curves shift to higher temperatures with increasing heating rates without intersecting, exhibiting key characteristics that validate their suitability for further kinetic analysis.

The isoconversional activation energy (E_α) of all deconvoluted peaks are shown in Fig. 8. For each peak, the minimum, average, and maximum values of E_α ($E_{\alpha,max}$, $E_{\alpha,min}$, and $E_{\alpha,avg}$) between conversions of 0.1 and 0.9, and the differences between the minimum and maximum E_α as percentages of the average E_α in this range, expressed as $E_{\alpha,diff}$, are provided in Table 2. Per the ICTAC kinetics committee guidelines, a deconvoluted peak can be considered to be a single-step process if its $E_{\alpha,diff}$ is less than 10%–20% [20].

From the values of $E_{\alpha,diff}$ in Table 2, it is seen that five out of seven deconvoluted peaks (peaks 1, 2, 3, 4, and 7) have $E_{\alpha,diff} < 20\%$ and can be considered to represent a single-step process. However, it is more likely that these peaks represent multiple processes limited by a single reaction or physical phenomenon, and insights into the underlying processes could theoretically be obtained from the $E_\alpha - \alpha$ dependence. For peaks 1 and 7, E_α decreases linearly with α – such phenomenon has been attributed to reversible reactions or a switch from chemical to diffusion-limited process in literature [25,52].

Peak 2 exhibits a near constant E_α for $0.1 < \alpha < 0.9$, suggesting an effectively single-step process. However, E_α rises sharply for $\alpha > 0.9$. Interestingly, the E_α profile of peak 3 for $\alpha < 0.1$ begins where peak 2's profile ends, showing a similar rapid increase. This continuity suggests that an intermediate step between peaks 2 and 3 may have been partially incorporated into both during the deconvolution process, which aimed to minimize the number of peaks. A similar transition in the E_α profile of a complex reaction with two steps with different

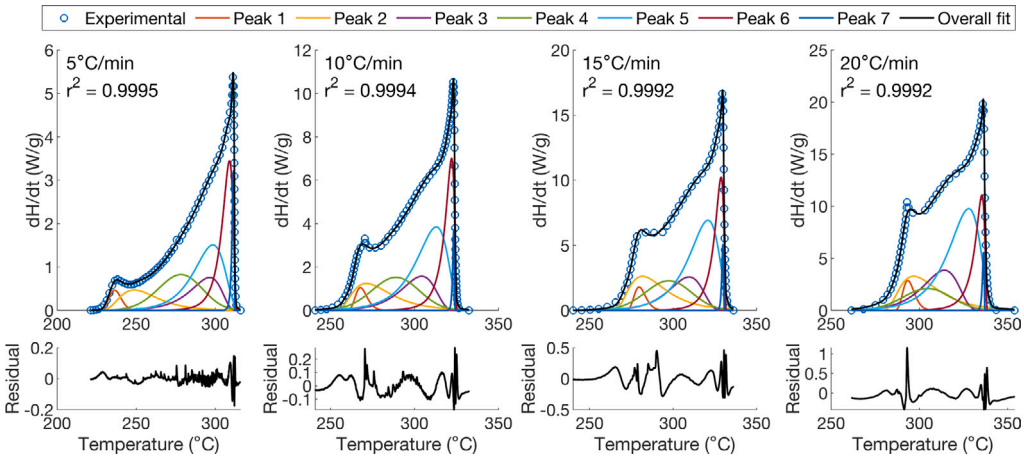

Fig. 4. Mathematical deconvolution of the exothermic segments of DSC curves of the munitions wastewater decomposition. The composite exotherms are resolved into seven peaks, the minimum number of peaks required for each peak to be defined by a reaction model with $r^2 \geq 0.95$.

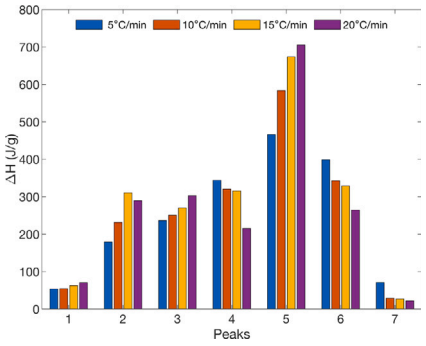

Fig. 5. Enthalpies of the deconvoluted peaks (ΔH_i) at experimental heating rates. Experimentally observed ΔH_{tot} for each heating rate can be recovered by summing the ΔH_i of the corresponding individual peaks. Noticeable patterns emerge in the dependence of ΔH_i on heating rate, which is expected due to the collective influence of reaction kinetics, residence times of gaseous intermediates, and heat transfer limitations.

activation energies is reported in [52]. This continuity in E_α profiles between adjacent peaks is observed in most transitions, with exceptions being the progressions from peak 1 to 2 and from peak 5 to 6.

A comparison of the E_α profile of peak 3 with characteristic $E_\alpha - \alpha$ dependencies [84] reveals that its initial stages show characteristics of competing reactions, while its final stages align with diffusion-controlled processes. Both competing reactions and diffusion-governed processes are features of the munitions wastewater decomposition due to the presence of multiple reacting species and heterogeneous reactions. The comparison indicates that while peak 3 has minor variations in E_α at relevant conversions, it is likely governed by different physicochemical processes across its conversion.

Peaks 4, 5, and 6 exhibit roughly linearly increasing values of E_α with α except at low or high conversions. This feature has been attributed to the gradual heating of the sample sequentially initiating low activation energy reactions first and high activation energy reactions at higher temperatures [56]. Alternatively, this phenomenon has also been attributed to competition between parallel reactions [85,86]. Both explanations suggest the presence of multiple reactions underlying these peaks, which for peaks 5 and 6, is evident from the variation in E_α values, provided in Table 2.

These discussions demonstrate that mathematical deconvolution using the Fraser-Suzuki function, followed by isoconversional analysis using the Friedman method, and examination of the $E_\alpha - \alpha$ dependence of deconvoluted peaks can provide a robust foundation for further deconvolution of a multi-step process into single-step processes. This approach could potentially lead to further breakdown of peaks 5 and 6, and the introduction of additional peaks between those exhibiting sharp E_α changes at extreme conversions and continuity in such changes between adjacent peaks. However, our focus is on reproducing the deconvoluted curves with empirical reaction models, which is discussed in the following section.

3.3. Model fitting on deconvoluted peaks

The frequency factor A and the reaction model $f(\alpha)$ of the deconvoluted peaks were determined simultaneously by employing the techniques outlined in Section 2.3.3. For each peak, the reaction model that yielded the lowest RMSE, which coincided with the highest r^2 value, was considered to be the governing mechanism.

Mechanistic model fits

The best mechanistic model fit results for the deconvoluted peaks are shown in Fig. 9. These include two Avrami-Erofeev nucleation models A1.5 and A4 (Eqs. (29) and (30)), and the exponent power second-order nucleation model E2 (equation (31)).

$$f_{\alpha,\,A1.5} = 1.5(1-\alpha)[-\ln(1-\alpha)]^{1/3} \tag{29}$$

$$f_{\alpha,\,A4} = 4(1-\alpha)[-\ln(1-\alpha)]^{3/4} \tag{30}$$

$$f_{\alpha,\,E2} = 0.5\alpha \tag{31}$$

The r^2 values of the mechanistic model fits range from 0.92 to 0.97, indicating that these models provide good fits to the deconvoluted peaks, but are likely insufficient for a predictive reduced-order model. Nevertheless, comparison of these fits with E_α profiles (Fig. 8) reveals that deviations between the model fits and deconvoluted curves correspond to clear shifts in the corresponding E_α profiles. For peaks with linear E_α profiles (peaks 1 and 7), the model fits align with deconvoluted curves at all conversions. For peaks with sharp variations and inflections in their E_α profiles (peaks 2 to 6), the model fits exhibit deviations at corresponding conversions. This observation supports the idea that E_α variations, even outside the $0.1 < \alpha < 0.9$ range, may indicate multiple underlying processes, even for effectively single-step peaks. Further investigation on this matter is beyond the scope of this work, however.

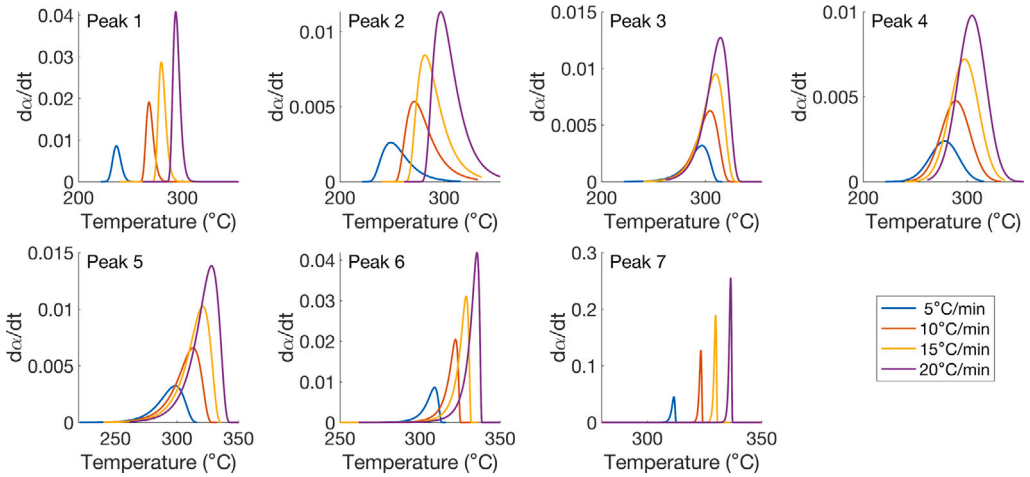

Fig. 6. Reaction rate ($d\alpha/dt$) curves of deconvoluted peaks at different heating rates.

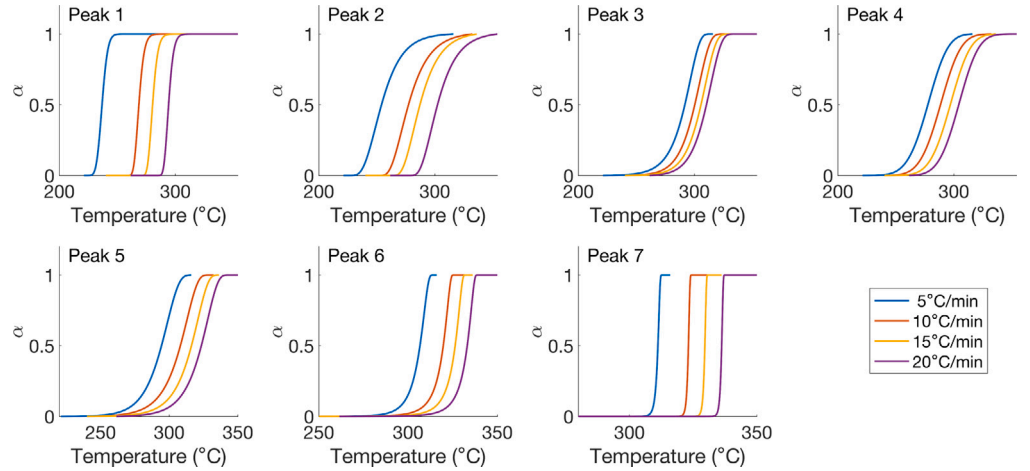

Fig. 7. Conversion (α) curves of deconvoluted peaks at different heating rates.

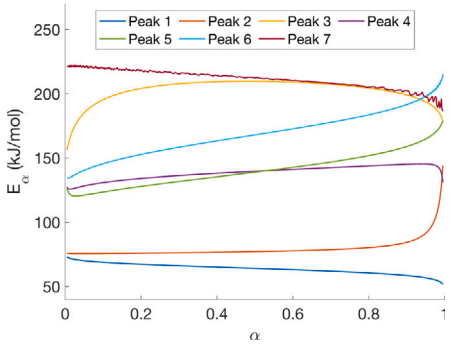

Fig. 8. E_α of deconvoluted peaks obtained with the Friedman method.

Empirical model fits

The best empirical models for all deconvoluted peaks are shown in Fig. 10. For peaks 1 to 4, best fits were obtained with two formulations of the autocatalytic Šesták-Berggren model (Eqs. (21) and (22)). Theoretically, Eq. (21) collapses to Eq. (22) when $c = 1$; the results therefore reflect the limitations of the optimization techniques to navigate the complex optimization landscape. Regardless, these empirical models capture the autocatalytic nature of the munitions wastewater decomposition. Peaks 5 to 7 are best fitted with the Šesták-Berggren model (Eq. (20)) proposed by Šesták and Berggren [68]. This model is capable of representing all forms of reaction models depending on the combination of parameters m, n, and p [25], allowing it to reproduce the complex behavior due to the superposition of multiple steps in peaks 5 and 6. While empirical model fits do not generally provide insights into the physicochemical processes of the reactions they represent, they offer better fits to the mathematically deconvoluted peaks to build a predictive model, which is the focus of this work.

Values of the coefficient of determination (r^2) for these fits vary between 0.968 and 0.997, indicating excellent fits. Visual inspection confirms good alignment between the deconvoluted peaks and empirical model fits. Therefore, we use the best-fitting empirical models in subsequent steps to build our reduced-order model.

3.4. Reduced-order model

The objective of the kinetic analysis performed so far, including mathematical deconvolution of the composite exotherm, followed by isoconversional analysis and model fitting on deconvoluted peaks, is to estimate the number of individual peaks required to model the wastewater decomposition, and obtain reliable initial values for kinetic parameters of these peaks. The kinetic parameters obtained so far were further optimized by minimizing the RMSE values between the deconvoluted and simulated peaks obtained by solving their $d\alpha/dt$ ODEs. The simulated $d\alpha/dt$ and α curves at all heating rates are compared with the deconvoluted ones in Figs. 11 and 12 respectively.

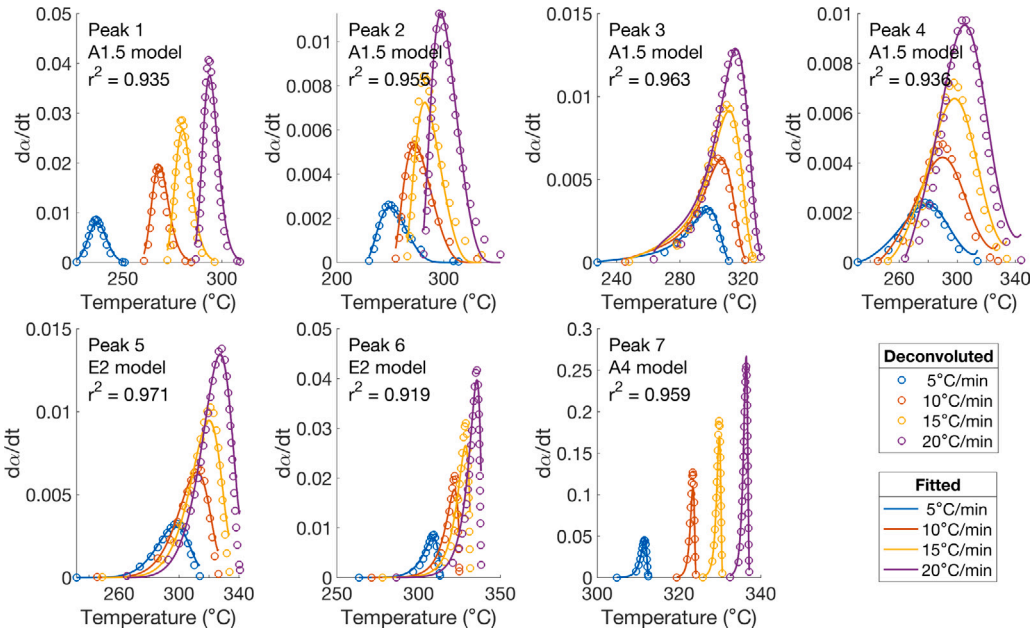

Fig. 9. The best mechanistic reaction model fits for the seven peaks comprising the composite exotherm of the munitions wastewater decomposition. All peaks are governed by nucleation mechanisms, including the Avrami-Erofeev and exponent power nucleation mechanisms.

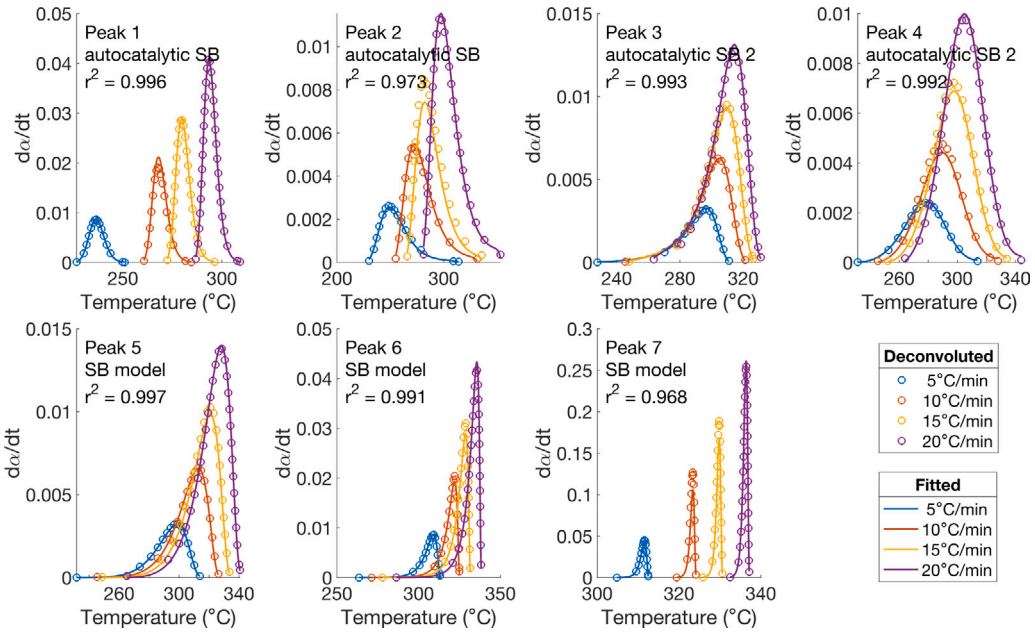

Fig. 10. The best empirical reaction mechanisms for the seven peaks comprising the composite exotherm of the munitions wastewater decomposition. Peaks 1 to 4 are represented by the autocatalytic Šesták-Berggren model, reflecting the autocatalytic nature of the wastewater decomposition. The multi-step processes captured in peaks 5 and 6 are best represented by the flexible Šesták-Berggren model.

Comparison of simulated curves with deconvoluted curves in Figs. 11 and 12 shows excellent agreement between the two for peaks 3, 4, 5, and 6. This demonstrates that the method employed here can reproduce even multi-step processes corresponding to peaks 5 and 6. However, the agreement is poorer for peak 1, particularly at the lowest heating rate of 5 °C/min. The T_{onset} for peak 1 at this heating rate is much lower than at other heating rates, which is a feature of the experimental data itself (Fig. 3). For peak 1, our model has not replicated this feature accurately. However, the same phenomenon is observed in the $d\alpha/dt$ curves of peak 7, for which the T_{onset} of the simulated curve at 5 °C/min aligns closely with that of the corresponding deconvoluted peak.

The simulated $d\alpha/dt$ curves of peak 2 have shoulders near their $T_{end\,set}$. The reason for this is found in the E_α profile of peak 2 (Fig. 8), which shows a sharp increase in E_α when α nears 1. Since the frequency factor for each peak is represented as a linear function of E_α according to Eq. (17), the pseudo-reaction represented by peak 2 becomes much faster in this region, resulting in the shoulders instead of the slowly decaying feature of the deconvoluted peak seen in Fig. 4. The likelihood of a minor single-step process between peaks 2 and 3 being incorporated in both was discussed earlier based on E_α profiles and mechanistic model fits of these peaks (Figs. 8 and 9 respectively). The shoulders observed in simulated curves of peak 2 are likely fitting artifacts/discrepancies resulting from this incorporation, a consequence of

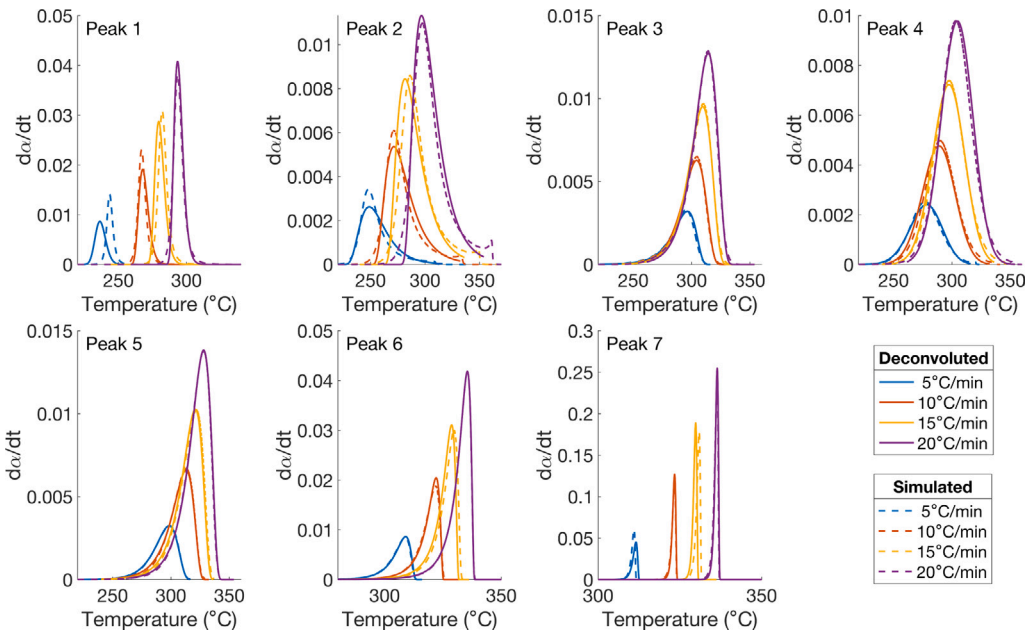

Fig. 11. Reaction rate ($d\alpha/dt$) curves of simulated peaks compared to those of deconvoluted peaks at different heating rates. Simulated peaks were obtained by ODE optimization of each peak's kinetic parameters (Eq. (18)) individually.

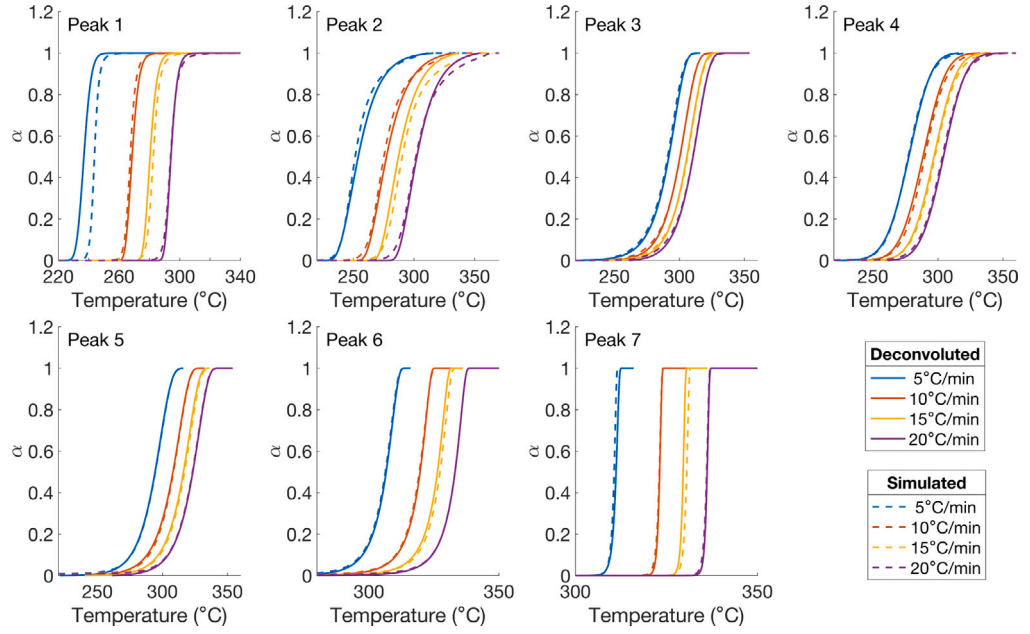

Fig. 12. Conversion (α) curves of simulated peaks compared to those of deconvoluted peaks at different heating rates. These curves were obtained from numerical integration of the corresponding $d\alpha/dt$ curves in Fig. 11.

our strategy to deconvolute the composite exotherm into as few peaks as possible. It is therefore probable that better fits can be obtained for peak 2 at all conversions if an additional peak is introduced during the deconvolution procedure.

Our reduced-order model is obtained by combining the simulated $d\alpha/dt$ curves of deconvoluted peaks with their weights to reproduce the composite exotherm of the wastewater decomposition. Fig. 13 shows the weights of all peaks obtained as $w_{i,\beta} = (\Delta H_i/\Delta H_{tot})_\beta$, where β is the heating rate. Table 3 presents the reaction rate expressions for all peaks, obtained by substituting the selected empirical reaction models into equation (28), and also lists all optimized parameter values required to solve the reduced-order model. The $E_\alpha - \alpha$ profiles of all peaks depicted in Fig. 8 are provided in Appendix A. While solving the model, the E_α values for these peaks at any step are determined through linear interpolation or extrapolation of the corresponding $E_\alpha - \alpha$ profile, based on the current α_i value. To prevent erroneous results at extreme conversions, the E_α value is set to be at least 100 J/mol for all α, and the pre-exponential factor A is set to be at least 1×10^{-3}.

Clear patterns emerge when observing the dependence of a peak's weight on the heating rate — the weights of six out of seven peaks increase or decrease in either a linear or a sigmoidal fashion. The weight of peak 2 increases linearly from 5 to 15 °C/min but remains stable from 15 to 20 °C/min. All these trends can be effectively captured in different sections of a modified "flat-top" Gaussian peak. Therefore, the weights of all peaks were modeled with Eq. (32), where i is the index of the deconvoluted peaks, β is the heating rate, and parameters a, b,

Table 3
Formulations of rate equations, and optimized values of parameters required to solve the reduced-order model of munitions wastewater decomposition. The E_α profiles of deconvoluted peaks reaction are shown in Fig. 8 and provided in Appendix A.

	Optimized parameters values							
Rates of deconvoluted peaks reactions	*a*	*b*	*c*	*f*	*m*	*n*	*p*	α_0
$\dot{\alpha}_1 = exp(a(f\ E_\alpha) + b)\ \exp\left(\frac{-f\ E_\alpha}{RT}\right) c\alpha^m(1-\alpha)^n$	2.6e−4	3.23	7.4e−4	0.75	1.1	1.2	–	9.9e−9
$\dot{\alpha}_2 = exp(a(f\ E_\alpha) + b)\ \exp\left(\frac{-f\ E_\alpha}{RT}\right) c\alpha^m(1-\alpha)^n$	3e−4	2.91	1.7e−5	0.76	0.89	2.1	–	1e−12
$\dot{\alpha}_3 = exp(a(f\ E_\alpha) + b)\ \exp\left(\frac{-f\ E_\alpha}{RT}\right) \alpha^m(1-\alpha)^n$	1.9e−4	0.29	–	0.94	0.61	1.1	–	1e−12
$\dot{\alpha}_4 = exp(a(f\ E_\alpha) + b)\ \exp\left(\frac{-f\ E_\alpha}{RT}\right) \alpha^m(1-\alpha)^n$	1.7e−4	1.76	–	0.98	0.72	1.3	–	1e−3
$\dot{\alpha}_5 = exp(a(f\ E_\alpha) + b)\ \exp\left(\frac{-f\ E_\alpha}{RT}\right) \alpha^m(1-\alpha)^n[-\ln(1-\alpha)]^p$	1.6e−4	2.5	–	1	−1.8	1.2	2.6	7.9e−3
$\dot{\alpha}_6 = exp(a(f\ E_\alpha) + b)\ \exp\left(\frac{-f\ E_\alpha}{RT}\right) \alpha^m(1-\alpha)^n[-\ln(1-\alpha)]^p$	1.8e−4	0.71	–	0.98	−1.5	1.1	2.6	3.6e−3
$\dot{\alpha}_7 = exp(a(f\ E_\alpha) + b)\ \exp\left(\frac{-f\ E_\alpha}{RT}\right) \alpha^m(1-\alpha)^n[-\ln(1-\alpha)]^p$	1.9e−4	0.02	–	0.77	−0.05	0.92	1.1	3e−12
Parameters for peaks' weights calculation	*a*	*b*	*c*	*d*	*e*			
Peak 1	0.0119	0.4022	0.0649	2.0398	0.0305			
Peak 2	0.1610	0.2898	0.3934	1.1502	0.0074			
Peak 3	0.0825	0.3901	0.0409	1.9300	0.1366			
Peak 4	0.2044	−0.0120	0.2339	2.7205	−0.0065			
Peak 5	0.3863	0.4997	0.4235	2.2731	0.0054			
Peak 6	0.2817	−0.1153	0.3964	1.0394	0.0712			
Peak 7	0.2111	−0.1088	0.1048	1.8917	0.0123			

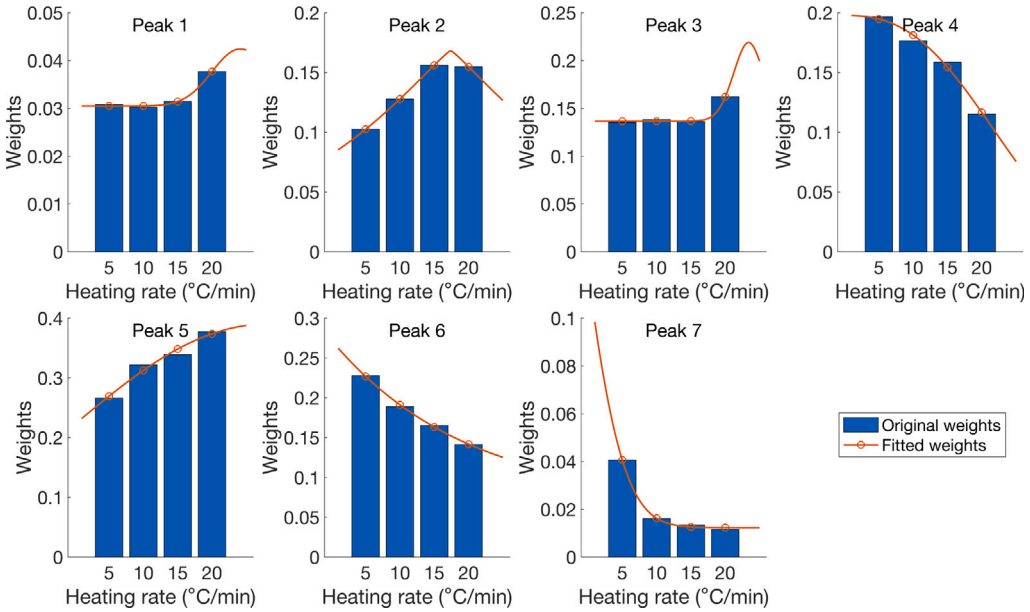

Fig. 13. Comparison of weights ($\Delta H_i/\Delta H_{tot}$) of deconvoluted peaks (bars) with weights simulated with a modified "flat-top" Gaussian function (plots with markers).

and c represent the amplitude, position, and standard deviation of the fitted function, respectively. Parameter d can introduce a flat-top in the fitted curve depending on its value, and parameter e represents the minimum weight of a peak. Eq. (32) reduces to the typical Gaussian function when $d = 2$ and $e = 0$.

$$w_{i,\beta} = a_i\ \exp\left[\frac{-(\beta - b_i)^d}{2c_i^2}\right] + e \tag{32}$$

Parameters a, b, c, d, and e for all peaks were simultaneously optimized using constrained pattern search method. Constraints imposed include lower and upper bounds based on experimental (deconvoluted) weights distributions, and non-linear constraints to enforce non-negative weights summing to 1 for each heating rate. As in previous steps, these bounds were imposed to prevent incorrect values without overly restricting the solution space. The modeled weights show good agreement with the deconvoluted peaks' weights across all experimental heating rates.

Fig. 14 compares the simulated overall $d\alpha/dt$ and α curves of the wastewater decomposition with the experimental ones, and also reports the r^2 values of the fits. The simulated $d\alpha/dt$ curves at 10 and 20 °C/min have r^2 values above 0.995, indicating excellent fits with the experimental results, which is confirmed by visual inspection of Fig. 14. However, the simulated $d\alpha/dt$ curves at 5 and 15 °C/min have r^2 values of 0.9201 and 0.9302 respectively, indicating comparatively poorer fits. The simulated curves at these heating rates do not align with the experimental ones in the initial stages of the exotherm, but have very good fits elsewhere. This is reflected in the fits between experimental and simulated conversion curves, which have $r^2 \geq 0.997$ in all cases. Such differences in r^2 values between differential ($d\alpha/dt$) and integral (α) data are typical, due to the smoothing of noise and fluctuations in differential data upon integration, and the cumulative nature of integral data.

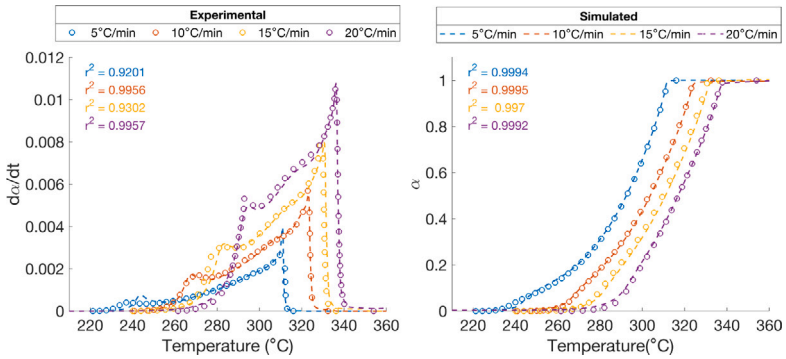

Fig. 14. Comparison of experimental and reduced-order model *(left)* $d\alpha/dt$ and *(right)* α curves of the exotherms of the munitions wastewater decomposition at different heating rates. Simulated curves were obtained by combining separately optimized kinetic and weights (contributions) parameters of individual deconvoluted peaks.

Table 4
A simplified reaction network representing the multi-step model of the munitions wastewater decomposition.

Step	Reaction
a	$H_2O\ (l) \xrightarrow{k_{H_2O}} H_2O\ (g)$
b	$AN \xrightarrow{k_{ion,eff}} AN^*$
c	$AN^* \xrightarrow{k_{rad}} AN^{**}$
d	$MAN \xrightarrow{barrierless} MAN^* + MAN^{**} + MAN^{***}$
1	$5\,AN^* + DMAN \xrightarrow{k_1} P_1$
2	$8\,AN^* + TMAN \xrightarrow{k_2} P_2$
3	$7\,AN^* + RDX + HMX \xrightarrow{k_3} P_3$
4	$AN^* \xrightarrow{k_4} P_4$
5	$2x\,AN^* + x\,MAN^* \xrightarrow{k_5} P_5$
6	$2y\,AN^{**} + y\,MAN^{**} \xrightarrow{k_6} P_6$
7	$2z\,AN^{**} + z\,MAN^{***} \xrightarrow{k_7} P_7$

We determine from visual inspection of Fig. 14 and reported r^2 values that our reduced-order model is capable of predicting the thermal decomposition behavior of the munitions wastewater with high fidelity, except at the lowest heating rate of 5 °C/min. However, we note that while the obtained solution is robust and provides a reliable description of the process, it does not necessarily represent the global optimum. It is also worth noting that these results have been obtained by analysis of the DSC data alone, without employing other analytical techniques or considering relevant mechanistic information. Moreover, further improvement might be gained by introducing additional peaks during the deconvolution procedure based on the E_α profiles and model fits of the deconvoluted peaks. This highlights the strength of our hierarchical approach in developing an accurate model of the wastewater decomposition, which is a complex process comprising many highly overlapped and mutually interacting steps.

3.5. Multi-step model

As the final step, we develop a multi-step model of the wastewater decomposition by expanding upon the reduced-order model and incorporating mechanistic information about the decomposition process. A simplified reaction network shown in Table 4 is constructed, and the multi-step model's prediction of the wastewater decomposition is obtained by solving this reaction network. The detailed procedure for developing this network is provided in the supplementary material Appendix A.

The reaction network consists of precursor reactions (a, b, c, and d) that affect the T_{onset} of the wastewater decomposition exotherms, but are assumed to not contribute to the experimental exothermic signals. The network also consists of semi-global reactions 1 to 7 comprising the wastewater decomposition assigned to deconvoluted peaks. Here, P_1 to P_7 represent the products of these semi-global reactions, and would include only CO_2, N_2, H_2O, and N_2O in case of ideal (complete) reactions, as illustrated in reactions SR1 to SR6 in the accompanying supplementary material. Parameters x, y, and z add to 1, preserving the stoichiometric coefficient of the overall reaction between AN and MAN (Eq. SR1).

Formulations of the reaction rate equations, and optimized values of all parameters required to solve the reaction network are tabulated in Table 5. Parameters to calculate peaks' weights are the same as the ones provided in Table 3. The formulations pertaining to the precursor reactions are derived in the supplementary material Appendix A.

The overall $d\alpha/dt$ and α curves from the multi-step model show good agreement with the experimental curves in Fig. 15. The r^2 values for these fits are comparable to those obtained from the reduced-order model, primarily because most of the optimized kinetic parameters are the same as their initial values obtained from the reduced-order model. This is consistent with prior findings in literature about final results depending considerably on the initial values [20,27], especially when optimizing a large number of parameters.

Theoretically, results from the multi-step model shown in Fig. 15 should show improvements over the results from the reduced-order model. However, the additional parameters in the multi-step model increase the optimization complexity and hinder convergence to the global optimum. Stochastic global optimization methods, despite their potential to address this issue, performed poorly compared to the pattern search method, and frequently returned objective functions many orders of magnitude higher, while being much more computationally expensive. This phenomenon occurs for any combination of moderately low E and high A values that results in sharp, tall peaks, and large errors.

These observations reinforce the ICTAC kinetics committee's recommendation to use as few steps as possible, and obtain reliable initial kinetic estimates, when modeling multi-step processes [20]. They also highlight the strength of our hierarchical approach in providing reliable estimates, and the effectiveness of using deterministic optimization techniques to efficiently refine them.

Fig. 16 shows the evolution of reactants in the wastewater, and products from its ideal decomposition at 20 °C/min as their temperature-dependent concentrations normalized by their initial and final concentrations, respectively. The ODE simulation of the multi-step model begins at 170 °C, the decomposition temperature of AN. This model predicts that N_2O is the initial product to form, which aligns with the results from analysis of emissions from the wastewater provided in [8], albeit from 0.5 MPa experiments. However, the concentration profiles also reflect the simplifying assumptions made in constructing the reaction network. For instance, although MAN decomposes at 251 °C, the model assumes its instantaneous, barrierless decomposition into MAN*, MAN**, and MAN***. While the AN* from AN dissociation is produced at temperatures above 200 °C, products of reactions

Table 5
Formulations of rate equations, and optimized values of parameters required to solve the multi-step model of munitions wastewater decomposition. Parameters for peaks' weights are provided in Table 3. The E_a profiles of deconvoluted peaks reaction are shown in Fig. 8 and provided in Appendix A.

	Optimized parameters values								
Rates of precursor reactions	$\ln(A)$	E(kJ/mol)	n	p	q	r	α_m	s	t
$\dot{\alpha}_a = A\mathrm{T}^n \exp\left(\frac{-E}{RT}\right)(1-\alpha)^p \frac{1}{\beta^q}$	24.2	110	−2.1	4.9	4.1	–	–	–	–
$\dot{\alpha}_b = k_{ion,eff}[AN]^p = k_{ion} \times k_{inh}\ [AN]^p$	–	–	–	3.4	–	–	–	–	–
$k_{ion} = A\mathrm{T}^n \exp\left(\frac{-E}{RT}\right)$	47.1	191	2	–	–	–	–	–	–
$k_{inh} = \left[\frac{1}{1+r\ \exp(\alpha_m - s\ \alpha_{H_2O})}\right]^t$	–	–	–	–	–	39.5	2.1	46.6	2.6
$\dot{\alpha}_c = A\mathrm{T}^n \exp\left(\frac{-E}{RT}\right)[AN^*]^q$	3.1	130	2.8	–	1	–	–	–	–
Rates of deconvoluted peaks reactions	a	b	c	f	m	n	p	$x/y/z$	α_0
$\dot{\alpha}_1 = exp(a(f\ E_\alpha)+b)\ \exp\left(\frac{-f\ E_\alpha}{RT}\right) c\alpha^m(1-\alpha)^n$	2.6e−4	3.23	7.4e−4	0.75	1.1	1.2	–	–	9.9e−9
$\dot{\alpha}_2 = exp(a(f\ E_\alpha)+b)\ \exp\left(\frac{-f\ E_\alpha}{RT}\right) c\alpha^m(1-\alpha)^n$	3e−4	2.91	1.7e−5	0.76	0.89	2.1	–	–	1e−12
$\dot{\alpha}_3 = exp(a(f\ E_\alpha)+b)\ \exp\left(\frac{-f\ E_\alpha}{RT}\right) \alpha^m(1-\alpha)^n$	1.9e−4	0.29	–	0.94	0.61	1.1	–	–	1e−12
$\dot{\alpha}_4 = exp(a(f\ E_\alpha)+b)\ \exp\left(\frac{-f\ E_\alpha}{RT}\right) \alpha^m(1-\alpha)^n$	1.7e−4	1.76	–	0.98	0.72	1.3	–	–	6.6e−4
$\dot{\alpha}_5 = exp(a(f\ E_\alpha)+b)\ \exp\left(\frac{-f\ E_\alpha}{RT}\right) \alpha^m(1-\alpha)^n[-\ln(1-\alpha)]^p$	1.6e−4	2.5	–	1	−1.8	1.2	2.6	0.64	8.2e−3
$\dot{\alpha}_6 = exp(a(f\ E_\alpha)+b)\ \exp\left(\frac{-f\ E_\alpha}{RT}\right) \alpha^m(1-\alpha)^n[-\ln(1-\alpha)]^p$	1.8e−4	0.71	–	0.98	−1.5	1.1	2.6	0.23	3.6e−3
$\dot{\alpha}_7 = exp(a(f\ E_\alpha)+b)\ \exp\left(\frac{-f\ E_\alpha}{RT}\right) \alpha^m(1-\alpha)^n[-\ln(1-\alpha)]^p$	1.9e−4	0.02	–	0.77	−0.05	0.92	1.1	0.14	3e-12

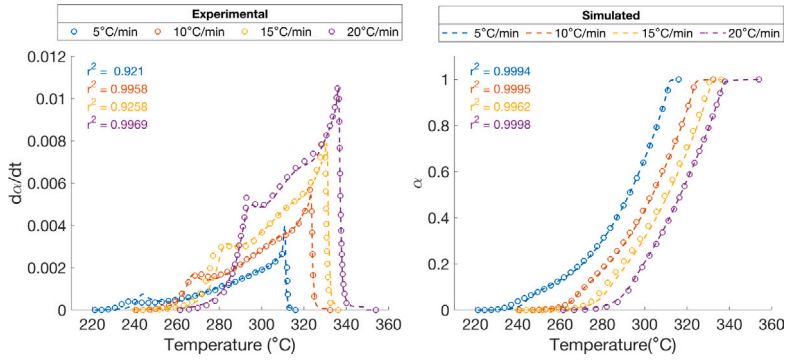

Fig. 15. Comparison of experimental and multi-step model *(left)* $d\alpha/dt$ and *(right)* α curves of the exotherms of the munitions wastewater decomposition at different heating rates. In the multi-step model, the peak profiles are influenced by both its kinetic parameters, and availability of and competition over reactants.

between AN* and fuel species shown in the reaction network only appear after the experimental T_{onset} of the exotherm. Their production is therefore governed by the kinetic parameters of the corresponding deconvoluted peaks, which potentially reflect the higher activation energies of decomposition of the participating fuel species.

Despite the challenges associated with kinetic modeling of complex multi-step processes, both the reduced-order and multi-step models accurately replicate the experimental exotherms and conversion curves of the wastewater decomposition. These results highlight the potential of our hierarchical approach for rigorous kinetic analysis of complex reactions with computationally efficient techniques, and without the need for reliable mechanistic information, experimental data from multiple analytical techniques, or knowledge of the sample composition.

4. Conclusions

A high-fidelity reduced-order model describing the thermal decomposition of ammonium nitrate (AN)-laden munitions wastewater was developed using a hierarchical approach to multi-step kinetic analysis. In doing so, this work demonstrated a rigorous framework for accurate empirical modeling of highly overlapped processes by analyzing experimental data from a single thermal analysis technique, without prior knowledge of sample composition or reaction behavior.

At the core of this framework is an iterative deconvolution procedure applied directly to experimental heat flow signals and residuals that provides reliable estimates for peak weights based on enthalpy contributions, and enables their independent modeling. Various reaction models are fitted to the resolved peaks individually, and resulting kinetic parameters for the best-fitting models are further refined and combined with the peak weights to construct the reduced-order model. This approach breaks the modeling process into manageable steps, enabling granular control and the application of computationally efficient techniques at each stage.

The reduced-order model was extended into a multi-step model by assigning semi-global reactions comprising the wastewater decomposition to individual peaks, based on alignment between peak characteristics and expected reaction behaviors. Predictions from the multi-step model regarding product evolution were consistent with limited experimental observations available, and both models achieved r^2 values of 0.996 or higher with experimental conversion curves.

It is important to clarify that good agreement with experimental results does not imply that the models identify definitive reaction pathways or exact kinetic parameters, nor is that the intent of this work. Instead, this work focuses on demonstrating a practical modeling approach for complex systems for which such details are inaccessible or difficult to obtain. By providing a detailed account of this methodology, we aim to offer a practical framework that could be adapted for kinetic

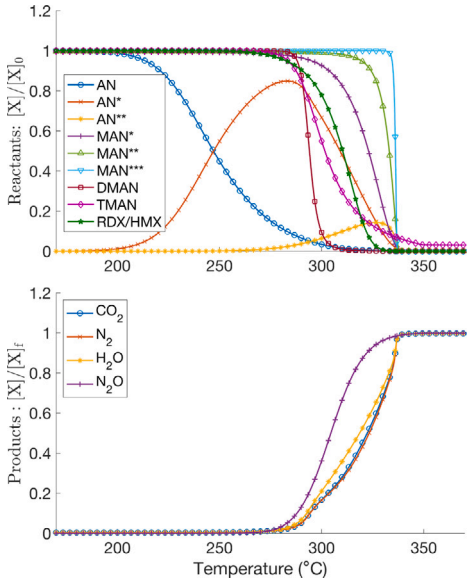

Fig. 16. Profiles of relative concentrations of *(top)* reactants and *(bottom)* products of ideal wastewater decomposition at 20 °C/min, as determined from the multi-step model.

analysis of other complex, multi-step systems. While the empirical nature of the models limits their utility for mechanistic interpretation, the results presented here demonstrate that the proposed methodology provides a strong foundation for its broader application to kinetically complex processes.

CRediT authorship contribution statement

Roshan Adhikari: Writing – review & editing, Writing – original draft, Validation, Software, Methodology, Investigation, Formal analysis, Conceptualization. **Jason Rabinovitch:** Writing – review & editing, Supervision, Conceptualization. **Nick Parziale:** Writing – review & editing, Supervision, Conceptualization. **Christos Christodoulatos:** Resources, Project administration, Funding acquisition, Supervision.

Declaration of competing interest

The authors declare that they have no known competing financial interests or personal relationships that could have appeared to influence the work reported in this paper.

Appendix A. Supplementary material

The supplementary material to this text details the procedure employed in developing the multi-step model, and provides the E_α profiles of deconvoluted peaks used in model simulations. It can be found in the online version at https://doi.org/10.1016/j.tca.2025.180038.

Data availability

Data will be made available on request.

References

[1] S. Chaturvedi, P.N. Dave, Review on thermal decomposition of ammonium nitrate, J. Energy Mater. 31 (2013) 1–26, http://dx.doi.org/10.1080/07370652.2011.573523.

[2] C. Oommen, S. Jain, Ammonium nitrate: A promising rocket propellant oxidizer, J. Hazard. Mater. 67 (1999) 253–281, http://dx.doi.org/10.1016/S0304-3894(99)00039-4.

[3] V.P. Sinditskii, V. Egorshev, A. Levshenkov, V.V. Serushkin, Ammonium nitrate: Combustion mechanism and the role of additives, Propellants, Explos. Pyrotech. 30 (2005) 269–280, http://dx.doi.org/10.1002/prep.200500017.

[4] M. Negovanović, L. Krič, S. Milanović, N. Đokić, N. Simić, Ammonium nitrate explosion hazards, Podzemn. Rad. 27 (2015) 49–63, http://dx.doi.org/10.5937/podrad1527049N.

[5] S. Ur Rehman, R. Ahmed, K. Ma, S. Xu, M.A. Aslam, H. Bi, J. Liu, J. Wang, Ammonium nitrate is a risk for environment: A case study of Beirut (Lebanon) chemical explosion and the effects on environment, Ecotoxicol. Env. Saf. 210 (2021) 111834, http://dx.doi.org/10.1016/j.ecoenv.2020.111834.

[6] M.E. Ortiz, A. Marco, N. Saiz, M. Lizana, Impact of ammonium nitrate on growth and survival of six European amphibians, Arch. Environ. Contam. Toxicol. 47 (2004) 234–239, http://dx.doi.org/10.1007/s00244-004-2296-x.

[7] M.E. Ortiz-Santaliestra, A. Marco, M.J. Fernández, M. Lizana, Influence of developmental stage on sensitivity to ammonium nitrate of aquatic stages of amphibians, Env. Toxicol. Chem. an Int. J. 25 (2006) 105–111, http://dx.doi.org/10.1897/05-023R.1.

[8] R. Adhikari, N. Parziale, T.-L. Su, W. Braida, C. Christodoulatos, Analysis of the thermal decomposition of munitions wastewater, Propellants, Explos. Pyrotech. 49 (2024) e202300139, http://dx.doi.org/10.1002/prep.202300139.

[9] J. Cox, D. Harrop, A. Head, The standard enthalpy of formation of ammonium nitrate and of the nitrate ion, J. Chem. Thermodyn. 11 (1979) 811–814, http://dx.doi.org/10.1016/0021-9614(79)90012-0.

[10] V.A. Medvedev, M.E. Efimov, P.J. Cerutti, R.M. McKay, L.H. Johnson, L.G. Hepler, Standard enthalpy of solution of ammonium nitrate in water at 298 K, Thermochim. Acta 23 (1978) 87–92, http://dx.doi.org/10.1016/0040-6031(78)85113-2.

[11] T. Cottrell, J. Gill, 392. The preparation and heats of combustion of some amine nitrates, J. Chem. Soc. (Resumed) (1951) 1798–1800, http://dx.doi.org/10.1039/JR9510001798.

[12] R. Meyer, J. Köhler, A. Homburg, Explosives, John Wiley & Sons, 2016.

[13] M.W. Chase, NIST-JANAF thermochemical tables 4th ed., J. Phys. Chem. Refernce Data (1998) 1529–1564, URL https://cir.nii.ac.jp/crid/1571698599286639488.

[14] K.R. Westerterp, E.J. Molga, No more runaways in fine chemical reactors, Ind. Eng. Chem. Res. 43 (2004) 4585–4594, http://dx.doi.org/10.1021/ie030725m.

[15] ANSYS, Inc., ANSYS chemkin-pro, 2023, Version 2023 R1.

[16] D.G. Goodwin, H.K. Moffat, I. Schoegl, R.L. Speth, B.W. Weber, Cantera: An object-oriented software toolkit for chemical kinetics, thermodynamics, and transport processes, 2023, http://dx.doi.org/10.5281/zenodo.8137090, version 3.0.0.

[17] B. Mosevitzky, A.G. Dana, G.E. Shter, G.S. Grader, Combustion simulations of aqueous urea ammonium nitrate monofuel at high pressures, Combust. Flame 166 (2016) 295–306, http://dx.doi.org/10.1016/j.combustflame.2016.01.030.

[18] W.A. Rosser, S.H. Inami, H. Wise, The kinetics of decomposition of liquid ammonium nitrate, J. Phys. Chem. 67 (1963) 1753–1757, http://dx.doi.org/10.1021/j100803a004.

[19] K.R. Brower, J.C. Oxley, M. Tewari, Evidence for homolytic decomposition of ammonium nitrate at high temperature, J. Phys. Chem. 93 (1989) 4029–4033, http://dx.doi.org/10.1021/j100347a033.

[20] S. Vyazovkin, A.K. Burnham, L. Favergeon, N. Koga, E. Moukhina, L.A. Pérez-Maqueda, N. Sbirrazzuoli, ICTAC kinetics committee recommendations for analysis of multi-step kinetics, Thermochim. Acta 689 (2020) 178597, http://dx.doi.org/10.1016/j.tca.2020.178597.

[21] P. Šimon, T. Dubaj, Z. Cibulková, Frequent flaws encountered in the manuscripts of kinetic papers, J. Therm. Anal. Calorim. 147 (2022) 10083–10088, http://dx.doi.org/10.1007/s10973-022-11436-y.

[22] A. Perejón, P.E. Sánchez-Jiménez, C. García-Garrido, L.A. Pérez-Maqueda, Kinetic study of complex processes composed of non-independent stages: Pyrolysis of natural rubber, Polym. Degrad. Stab. 188 (2021) 109590, http://dx.doi.org/10.1016/j.polymdegradstab.2021.109590.

[23] S.J. Klippenstein, V.S. Pande, D.G. Truhlar, Chemical kinetics and mechanisms of complex systems: A perspective on recent theoretical advances, J. Am. Chem. Soc. 136 (2014) 528–546, http://dx.doi.org/10.1021/ja408723a.

[24] N. Sbirrazzuoli, Kinetic analysis of complex chemical reactions by coupling model-free and model-fitting analysis, Thermochim. Acta 719 (2023) 179416, http://dx.doi.org/10.1016/j.tca.2022.179416.

[25] S. Vyazovkin, A.K. Burnham, J.M. Criado, L.A. Pérez-Maqueda, C. Popescu, N. Sbirrazzuoli, ICTAC kinetics committee recommendations for performing kinetic computations on thermal analysis data, Thermochim. Acta 520 (2011) 1–19, http://dx.doi.org/10.1016/j.tca.2011.03.034.

[26] J.C.G. da Silva, J.G. de Albuquerque, W.V. de Araujo Galdino, R.F. de Sena, S.L.F. Andersen, Single-step and multi-step thermokinetic study – deconvolution method as a simple pathway for describe properly the biomass pyrolysis for energy conversion, Energy Convers. Manag. 209 (2020) 112653, http://dx.doi.org/10.1016/j.enconman.2020.112653.

[27] N.V. Muravyev, A.N. Pivkina, N. Koga, Critical appraisal of kinetic calculation methods applied to overlapping multistep reactions, Molecules 24 (2019) 2298, http://dx.doi.org/10.3390/molecules24122298.

[28] N.V. Muravyev, N. Koga, D.B. Meerov, A.N. Pivkina, Kinetic analysis of overlapping multistep thermal decomposition comprising exothermic and endothermic processes: thermolysis of ammonium dinitramide, Phys. Chem. Chem. Phys. 19 (2017) 3254–3264, http://dx.doi.org/10.1039/C6CP08218A.

[29] M. Nakano, T. Wada, N. Koga, Exothermic behavior of thermal decomposition of sodium percarbonate: Kinetic deconvolution of successive endothermic and exothermic processes, J. Phys. Chem. A 119 (2015) 9761–9769, http://dx.doi.org/10.1021/acs.jpca.5b07044.

[30] J.C. Pinto, M.W. Lobao, A.L. Alberton, M. Schwaab, M. Embirucu, S. Vieira de Melo, Critical analysis of kinetic modeling procedures, Int. J. Chem. React. Eng. 9 (2011) http://dx.doi.org/10.2202/1542-6580.2796.

[31] O. Rodionova, A. Pomerantsev, Estimating the parameters of the arrhenius equation, Kinet. Catal. 46 (2005) 305–308, http://dx.doi.org/10.1007/s10975-005-0077-9.

[32] A. Perejón, P.E. Sánchez-Jiménez, J.M. Criado, L.A. Pérez-Maqueda, Kinetic analysis of complex solid-state reactions. A new deconvolution procedure, J. Phys. Chem. B 115 (2011) 1780–1791, http://dx.doi.org/10.1021/jp110895z.

[33] H. Liu, N. Lyczko, A. Nzihou, C. Eskicioglu, Phosphorus extracted municipal sludge-derived hydrochar as a potential solid fuel: Effects of acidic leaching and combustion mechanism, Chem. Eng. J. 473 (2023) 145191, http://dx.doi.org/10.1016/j.cej.2023.145191.

[34] S. Wang, Y. Wen, Z. Shi, L. Niedzwiecki, M. Baranowski, M. Czerep, W. Mu, H.P. Kruczek, P.G. Jönsson, W. Yang, Effect of hydrothermal carbonization pretreatment on the pyrolysis behavior of the digestate of agricultural waste: A view on kinetics and thermodynamics, Chem. Eng. J. 431 (2022) 133881, http://dx.doi.org/10.1016/j.cej.2021.133881.

[35] M. El Hazzat, A. Sifou, S. Arsalane, A. El Hamidi, Novel approach to thermal degradation kinetics of gypsum: Application of peak deconvolution and model-free isoconversional method, J. Therm. Anal. Calorim. 140 (2020) 657–671, http://dx.doi.org/10.1007/s10973-019-08885-3.

[36] M. El Hazzat, A. Sifou, S. Arsalane, Complex thermal kinetic study of calcium phosphate biomaterial $CaHPO_4$ using the asymmetric deconvolution approach, J. Therm. Anal. Calorim. 147 (2022) 9747–9761, http://dx.doi.org/10.1007/s10973-022-11229-3.

[37] Y. Zushi, S. Iwasaki, N. Koga, Physico-geometrical kinetics of the thermal dehydration of sodium carbonate monohydrate as a compacted composite of inorganic hydrate comprising crystalline particles and matrix, Phys. Chem. Chem. Phys. 24 (2022) 15736–15748, http://dx.doi.org/10.1039/D2CP01948E.

[38] S. Pinzi, C. Buratti, P. Bartocci, G. Marseglia, F. Fantozzi, M. Barbanera, A simplified method for kinetic modeling of coffee silver skin pyrolysis by coupling pseudo-components peaks deconvolution analysis and model free-isoconversional methods, Fuel 278 (2020) 118260, http://dx.doi.org/10.1016/j.fuel.2020.118260.

[39] A.L. Pomerantsev, A.V. Kutsenova, O.Y. Rodionova, Kinetic analysis of non-isothermal solid-state reactions: multi-stage modeling without assumptions in the reaction mechanism, Phys. Chem. Chem. Phys. 19 (2017) 3606–3615, http://dx.doi.org/10.1039/C6CP07529K.

[40] C. Sronsri, B. Boonchom, Deconvolution technique for the kinetic analysis of a complex reaction and the related thermodynamic functions of the formation of $LiMn_{0.90}Co_{0.05}Mg_{0.05}PO_4$, Chem. Phys. Lett. 690 (2017) 116–128, http://dx.doi.org/10.1016/j.cplett.2017.10.045.

[41] C. García-Garrido, P.E. Sánchez-Jiménez, L.A. Pérez-Maqueda, A. Perejón, J.M. Criado, Combined TGA-MS kinetic analysis of multistep processes. Thermal decomposition and ceramification of polysilazane and polysiloxane preceramic polymers, Phys. Chem. Chem. Phys. 18 (2016) 29348–29360, http://dx.doi.org/10.1039/C6CP03677E.

[42] M. Wesolowski, E. Leyk, Coupled and simultaneous thermal analysis techniques in the study of pharmaceuticals, Pharmaceutics 15 (2023) 1596, http://dx.doi.org/10.3390/pharmaceutics15061596.

[43] E. Yao, S. Xu, F. Zhao, T. Huang, H. Li, N. Zhao, J. Yi, Y. Yang, C. Wang, Study on thermal decomposition behavior, gaseous products, and kinetic analysis of bis-(dimethylglyoximato) nickel (II) complex using TG-DSC-FTIR-MS technique, Catalysts 10 (2020) 331, http://dx.doi.org/10.3390/catal10030331.

[44] D. Skala, M. Sokić, J. Tomić, H. Kopsch, Kinetic analysis of consecutive reactions using TG and DSC techniques: Theory and application, J. Therm. Anal. 35 (1989) 1441–1458, http://dx.doi.org/10.1007/BF01912921.

[45] H. Schmid, N. Eisenreich, C. Krause, A. Pfeil, Analysis of complex thermoanalytical curves: The thermodynamic and kinetic parameters of isopropylammonium nitrate, J. Therm. Anal. 35 (1989) 569–576, http://dx.doi.org/10.1007/BF01904458.

[46] S. Vyazovkin, C. Wight, Model-free and model-fitting approaches to kinetic analysis of isothermal and nonisothermal data, Thermochim. Acta 340–341 (1999) 53–68, http://dx.doi.org/10.1016/S0040-6031(99)00253-1.

[47] A.G. Dana, G. Tvil, L. Winter, G.E. Shter, G.S. Grader, Pressure effect on the combustion of aqueous urea ammonium nitrate alternative fuel, Fuel 159 (2015) 500–507, http://dx.doi.org/10.1016/j.fuel.2015.06.099.

[48] A.G. Dana, B. Mosevitzky, G. Tvil, M. Epstein, G.E. Shter, G.S. Grader, Flow reactor combustion of aqueous urea ammonium nitrate fuel, Energy & Fuels 30 (2016) 2474–2477, http://dx.doi.org/10.1021/acs.energyfuels.6b00115.

[49] S. Vyazovkin, K. Chrissafis, M.L. Di Lorenzo, N. Koga, M. Pijolat, B. Roduit, N. Sbirrazzuoli, J.J. Suñol, ICTAC kinetics committee recommendations for collecting experimental thermal analysis data for kinetic computations, Thermochim. Acta 590 (2014) 1–23, http://dx.doi.org/10.1016/j.tca.2014.05.036.

[50] S. Vyazovkin, Kinetic effects of pressure on decomposition of solids, Int. Rev. Phys. Chem. 39 (2020) 35–66, http://dx.doi.org/10.1080/0144235X.2019.1691319.

[51] M.R. Wright, Introduction to Chemical Kinetics, John Wiley & Sons, 2005.

[52] S. Vyazovkin, A time to search: finding the meaning of variable activation energy, Phys. Chem. Chem. Phys. 18 (2016) 18643–18656, http://dx.doi.org/10.1039/C6CP02491B.

[53] F. Zhang, Z.-T. Liu, P. Du, Thermal decomposition kinetics of nitroguanidine propellant under different pressures, Propellants, Explos. Pyrotech. 43 (2018) 390–397, http://dx.doi.org/10.1002/prep.201700217.

[54] K.J. Laidler, The development of the Arrhenius equation, J. Chem. Educ. 61 (1984) 494, http://dx.doi.org/10.1021/ed061p494.

[55] J. Martin, Kinetic analysis of two DSC peaks in the curing of an unsaturated polyester resin catalyzed with methylethylketone peroxide and cobalt octoate, Polym. Eng. Sci. 47 (2007) 62–70, http://dx.doi.org/10.1002/pen.20667.

[56] J. Wang, M.-P.G. Laborie, M.P. Wolcott, Comparison of model-free kinetic methods for modeling the cure kinetics of commercial phenol–formaldehyde resins, Thermochim. Acta 439 (2005) 68–73, http://dx.doi.org/10.1016/j.tca.2005.09.001.

[57] R.D. Fraser, E. Suzuki, Resolution of overlapping absorption bands by least squares procedures, Anal. Chem. 38 (1966) 1770–1773, http://dx.doi.org/10.1021/ac60244a038.

[58] R.D. Fraser, E. Suzuki, Resolution of overlapping bands: Functions for simulating band shapes, Anal. Chem. 41 (1969) 37–39, http://dx.doi.org/10.1021/ac60270a007.

[59] N. Koga, Y. Goshi, S. Yamada, L.A. Pérez-Maqueda, Kinetic approach to partially overlapped thermal decomposition processes: Co-precipitated zinc carbonates, J. Therm. Anal. Calorim. 111 (2013) 1463–1474, http://dx.doi.org/10.1007/s10973-012-2500-6.

[60] R.H. Byrd, M.E. Hribar, J. Nocedal, An interior point algorithm for large-scale nonlinear programming, SIAM J. Optim. 9 (1999) 877–900, http://dx.doi.org/10.1137/S1052623497325107.

[61] H.L. Friedman, Kinetics of thermal degradation of char-forming plastics from thermogravimetry. Application to a phenolic plastic, J. Polym. Sci. Part C: Polym. Symp. 6 (1964) 183–195, http://dx.doi.org/10.1002/polc.5070060121.

[62] S. Sobek, S. Werle, Isoconversional determination of the apparent reaction models governing pyrolysis of wood, straw and sewage sludge, with an approach to rate modelling, Renew. Energy 161 (2020) 972–987, http://dx.doi.org/10.1016/j.renene.2020.07.112.

[63] A.K. Burnham, R.L. Braun, H.R. Gregg, A.M. Samoun, Comparison of methods for measuring kerogen pyrolysis rates and fitting kinetic parameters, Energy & Fuels 1 (1987) 452–458, http://dx.doi.org/10.1021/ef00006a001.

[64] F.J. Gotor, J.M. Criado, J. Malek, N. Koga, Kinetic analysis of solid-state reactions: The universality of master plots for analyzing isothermal and non-isothermal experiments, J. Phys. Chem. A 104 (2000) 10777–10782, http://dx.doi.org/10.1021/jp0022205.

[65] P.J. Barrie, The mathematical origins of the kinetic compensation effect: 1. the effect of random experimental errors, Phys. Chem. Chem. Phys. 14 (2012) 318–326, http://dx.doi.org/10.1039/C1CP22666E.

[66] N. Koga, J. Šesták, Kinetic compensation effect as a mathematical consequence of the exponential rate constant, Thermochim. Acta 182 (1991) 201–208, http://dx.doi.org/10.1016/0040-6031(91)80005-4.

[67] K. Açıkalın, Determination of kinetic triplet, thermal degradation behaviour and thermodynamic properties for pyrolysis of a lignocellulosic biomass, Bioresour. Technol. 337 (2021) 125438, http://dx.doi.org/10.1016/j.biortech.2021.125438.

[68] J. Šesták, G. Berggren, Study of the kinetics of the mechanism of solid-state reactions at increasing temperatures, Thermochim. Acta 3 (1971) 1–12, http://dx.doi.org/10.1016/0040-6031(71)85051-7.

[69] J. Sestak, Science of Heat and Thermophysical Studies: A Generalized Approach To Thermal Analysis, Elsevier, 2005.

[70] N. Akulov, Basics of Chemical Dynamics, Moscow State University, Moscow, 1940, p. 56.

[71] M. Avrami, Kinetics of phase change. I general theory, J. Chem. Phys. 7 (1939) 1103, http://dx.doi.org/10.1063/1.1750380.

[72] I. Arkhangel'Skii, A. Dunaev, I. Makarenko, N. Tikhonov, S. Belyaev, A. Tarasov, Non-isothermal kinetic methods, 2013, Workb. laboratory manual. Max Planck research library for history development knowledge. Ger. Ed. Open Access Berlin.

[73] J.A. Nelder, R. Mead, A simplex method for function minimization, Comput. J. 7 (1965) 308–313, http://dx.doi.org/10.1093/comjnl/7.4.308.

[74] R. Hooke, T.A. Jeeves, Direct Search solution of numerical and statistical problems, J. ACM (JACM) 8 (1961) 212–229, http://dx.doi.org/10.1145/321062.321069.

[75] V. Torczon, On the convergence of pattern search algorithms, SIAM J. Optim. 7 (1997) 1–25, http://dx.doi.org/10.1137/S1052623493250780.

[76] A. Ambekar, J.J. Yoh, Chemical kinetics of multi-component pyrotechnics and mechanistic deconvolution of variable activation energy, Proc. Combust. Inst. 37 (2018) 3193–3201, http://dx.doi.org/10.1016/j.proci.2018.05.142.

[77] Y.-I. Izato, A. Miyake, Kinetic analysis of the thermal decomposition of liquid ammonium nitrate based on thermal analysis and detailed reaction simulations, J. Therm. Anal. Calorim. 134 (2018) 813–823, http://dx.doi.org/10.1007/s10973-018-7322-8.

[78] T.P. Russell, T.B. Brill, Thermal decomposition of energetic materials 31 — fast thermolysis of ammonium nitrate, ethylenediammonium dinitrate and hydrazinium nitrate and the relationship to the burning rate, Combust. Flame 76 (1989) 393–401, http://dx.doi.org/10.1016/0010-2180(89)90120-X.

[79] D.G. Patil, S.R. Jain, T.B. Brill, Thermal decomposition of energetic materials 56. On the fast thermolysis mechanism of ammonium nitrate and its mixtures with magnesium and carbon, Propellants, Explos. Pyrotech. 17 (1992) 99–105, http://dx.doi.org/10.1002/prep.19920170302.

[80] F. Cotton, G. Wilkinson, Advanced inorganic chemistry: A comprehensive text, 1972.

[81] Y.-I. Izato, A. Miyake, S. Date, Combustion characteristics of ammonium nitrate and carbon mixtures based on a thermal decomposition mechanism, Propellants, Explos. Pyrotech. 38 (2013) 129–135, http://dx.doi.org/10.1002/prep.201100106.

[82] E. García, D. Sánchez-Rodríguez, J.P. López-Olmedo, J. Farjas, P. Roura, The effect of volatiles on the measurement of the reaction heat by differential scanning calorimetry, J. Therm. Anal. Calorim. 121 (2015) 187–194, http://dx.doi.org/10.1007/s10973-015-4465-8.

[83] Q. Chen, R. Yang, B. Zhao, Y. Li, S. Wang, H. Wu, Y. Zhuo, C. Chen, Investigation of heat of biomass pyrolysis and secondary reactions by simultaneous thermogravimetry and differential scanning calorimetry, Fuel 134 (2014) 467–476, http://dx.doi.org/10.1016/j.fuel.2014.05.092.

[84] S. Vyazovkin, C. Wight, Kinetics in solids, Annu. Rev. Phys. Chem. 48 (1997) 125–149, http://dx.doi.org/10.1146/annurev.physchem.48.1.125.

[85] S. Vyazovkin, A. Lesnikovich, Error in determining activation energy caused by the wrong choice of process model, Thermochim. Acta 165 (1990) 11–15, http://dx.doi.org/10.1016/0040-6031(90)80201-9.

[86] G. He, B. Riedl, A. Aït-Kadi, Model-free kinetics: Curing behavior of phenol formaldehyde resins by differential scanning calorimetry, J. Appl. Polym. Sci. 87 (2003) 433–440, http://dx.doi.org/10.1002/app.11378.